CORRECTED 19 JULY 2017; SEE ERRATUM

SCIENCE TRANSLATIONAL MEDICINE | RESEARCH ARTICLE

CANCER

Neoadjuvant chemotherapy induces breast cancer metastasis through a TMEM-mediated mechanism

George S. Karagiannis,[1,2]* Jessica M. Pastoriza,[1,3] Yarong Wang,[1,2,4] Allison S. Harney,[1,2,4,5] David Entenberg,[1,2,4] Jeanine Pignatelli,[1] Ved P. Sharma,[1,4] Emily A. Xue,[1] Esther Cheng,[6] Timothy M. D'Alfonso,[6] Joan G. Jones,[1,2,7,8] Jesus Anampa,[9] Thomas E. Rohan,[8] Joseph A. Sparano,[9] John S. Condeelis,[1,2,4]* Maja H. Oktay[1,4,7]*

Breast cancer cells disseminate through TIE2/MENA^{Calc}/MENA^{INV}-dependent cancer cell intravasation sites, called tumor microenvironment of metastasis (TMEM), which are clinically validated as prognostic markers of metastasis in breast cancer patients. Using fixed tissue and intravital imaging of a PyMT murine model and patient-derived xenografts, we show that chemotherapy increases the density and activity of TMEM sites and Mena expression and promotes distant metastasis. Moreover, in the residual breast cancers of patients treated with neoadjuvant paclitaxel after doxorubicin plus cyclophosphamide, TMEM score and its mechanistically connected MENA^{INV} isoform expression pattern were both increased, suggesting that chemotherapy, despite decreasing tumor size, increases the risk of metastatic dissemination. Chemotherapy-induced TMEM activity and cancer cell dissemination were reversed by either administration of the TIE2 inhibitor rebastinib or knockdown of the *MENA* gene. Our results indicate that TMEM score increases and MENA isoform expression pattern changes with chemotherapy and can be used in predicting prometastatic changes in response to chemotherapy. Furthermore, inhibitors of TMEM function may improve clinical benefits of chemotherapy in the neoadjuvant setting or in metastatic disease.

INTRODUCTION

Breast cancer cell intravasation and dissemination occur at microanatomical structures called tumor microenvironment of metastasis (TMEM). Each TMEM is composed of three different cell types in direct physical contact: a tumor cell expressing the actin-regulatory protein Mammalian-enabled (MENA), a perivascular macrophage, and an endothelial cell (*1*, *2*). TMEM sites have been identified in mouse and human mammary carcinomas, and their density correlates with metastatic outcome in breast cancer patients (*3*–*5*). High-resolution intravital imaging (IVI) of murine primary breast tumors revealed that TMEM sites induce local and transient dissociation of endothelial cell junctions, through which migratory cancer cells may intravasate and disseminate to secondary sites (*1*). TMEM-dependent vascular permeability is localized and is mediated by vascular endothelial growth factor–A (VEGF-A) release from the TMEM-bound macrophages, which express the angiopoietin receptor TIE2 (*1*).

Randomized prospective studies indicate that addition of paclitaxel into the preoperative neoadjuvant chemotherapy (NAC) regimen increases the rate of pathologic complete response (pCR) but paradoxically does not improve the overall survival (*6*, *7*). It has also been shown that taxane-based chemotherapies promote tumor regrowth by inducing angiogenesis. In particular, they mobilize bone marrow–derived mesenchymal and endothelial progenitors and CD11b$^+$ myeloid cells, including TIE2$^+$ monocytes, into the primary tumor microenvironment (*8*–*13*). TIE2$^+$ monocyte progenitors transform into TIE2^{hi} macrophages, which associate with newly constructed tumor blood vessels and promote tumor regrowth (*14*, *15*). As stated before, TIE2^{hi} macrophages are also critical constituents of the functional TMEM sites, where they mediate VEGF-A–induced blood vessel permeability and tumor cell intravasation.

TMEM-dependent vascular permeability is necessary but not sufficient for tumor cell intravasation, because intravasation also requires the presence of discohesive, migratory cancer cells (*1*, *16*–*18*). These migratory cells express relatively large amounts of invasive, chemotactic prometastatic MENA isoforms (*19*), such as the MENA^{INV} isoform, and relatively smaller amounts of the antimetastatic MENA isoform, MENA11a (*18*–*26*). MENA^{INV} expression is switched on in invasive tumor cells by NOTCH-mediated macrophage contact and signaling (*27*). Because paclitaxel induces an influx of macrophages into the primary tumor, and these are required for TMEM assembly and function (*1*, *2*, *20*, *21*, *28*, *29*), we hypothesized that preoperative chemotherapy may increase the density and the activity of TMEM sites, as well as expression of invasion-promoting MENA isoforms within the primary tumor, and consequently induce cancer cell dissemination and distant metastasis while at the same time reducing cancer burden. Such a side effect would diminish the clinical benefit of NAC and would need to be blocked by inhibitors of TMEM function. Here, we tested this hypothesis by using fixed tissue and IVI of mouse mammary tumor virus–polyoma middle T antigen (MMTV-PyMT) murine models and patient-derived xenografts (PDXs), as well as pre- and post-NAC (paclitaxel followed by doxorubicin plus cyclophosphamide) breast cancer tissue samples from human patients.

RESULTS

Paclitaxel delays tumor growth but increases TMEM assembly in breast cancer

Because chemotherapy induces recruitment of endothelial progenitors and TIE2$^+$ monocyte progenitors into the tumor (*10*, *11*, *30*), and we

[1]Department of Anatomy and Structural Biology, Albert Einstein College of Medicine, Bronx, NY 10461, USA. [2]Integrated Imaging Program, Albert Einstein College of Medicine, Bronx, NY 10461, USA. [3]Department of Surgery, Montefiore Medical Center, Albert Einstein College of Medicine, Bronx, NY 10467, USA. [4]Gruss-Lipper Biophotonics Center, Albert Einstein College of Medicine, Bronx, NY 10461, USA. [5]Department of Radiology, Albert Einstein College of Medicine, Bronx, NY 10461, USA. [6]Department of Pathology and Laboratory Medicine, Weill Cornell Medicine, New York, NY 10065, USA. [7]Department of Pathology, Montefiore Medical Center, Bronx, NY 10467, USA. [8]Department of Epidemiology and Population Health, Albert Einstein College of Medicine, Bronx, NY 10461, USA. [9]Department of Oncology, Montefiore Medical Center, Albert Einstein College of Medicine, Bronx, NY 10467, USA.
*Corresponding author. Email: georgios.karagiannis@einstein.yu.edu (G.S.K.); john.condeelis@einstein.yu.edu (J.S.C.); maja.oktay@einstein.yu.edu (M.H.O.)

have previously demonstrated that TIE2^{hi} macrophages are required for TMEM-mediated cancer cell intravasation (*1*), we examined the possibility that neoadjuvant paclitaxel promotes TMEM assembly and cancer cell dissemination and metastasis. We addressed this hypothesis in the following breast carcinoma models: (i) transgenic MMTV-PyMT mice bearing spontaneous breast tumors, (ii) friend virus B (FVB) mice transplanted orthotopically with tumors from MMTV-PyMT donors, and (iii) two PDX models, the HT17 and HT33, developed previously in our laboratory (*31*). Animals were treated with paclitaxel (10 mg/kg) every 5 days, three times in total (Fig. 1A). The number of animals per group is shown in Fig. 1B. After sacrificing the animals, we evaluated tumor growth, TIE2^{hi} macrophage recruitment, and TMEM assembly. Treatment of all groups began at the early carcinoma stage (tumor size of ~0.3 cm diameter), when there was minimal or absent necrosis (fig. S1). We chose to work with early-stage PyMT mouse mammary carcinoma model, because it more accurately reflects clinically relevant scenarios, where most women present with small-sized tumors of <2 cm (*32*). At the end of treatment, all tumors were histologically classified as invasive carcinomas (fig. S1). Although paclitaxel-treated tumors showed delayed tumor growth (Fig. 1C), they revealed a two- to threefold higher TMEM score ($P < 0.001$) compared to nontreated controls in all the experimental models (Fig. 1, D and E).

Paclitaxel increases the infiltration of perivascular TIE2^{hi}/VEGF^{hi} macrophages in the primary breast cancer microenvironment

To explain the mechanism of increased TMEM assembly upon administering chemotherapy in breast tumors, we investigated whether paclitaxel affects intratumoral macrophage density, as previously suggested (*33*). We found a significant increase ($P < 0.01$) in the percentage of macrophage-specific IBA1$^+$ area in paclitaxel-treated mice in all transplantation models, but not in the PyMT spontaneous model (fig. S2A). Consistently, the absolute number of IBA1$^+$ cells was significantly increased ($P < 0.001$) in the paclitaxel-treated HT17 xenograft but not in the PyMT spontaneous model, when quantified either over the entire tissue (fig. S2B) or only in the perivascular niche (Fig. 1F), where TMEM structures are located.

The functional TMEM sites contain TIE2^{hi}/VEGF^{hi} macrophages and invasive tumor cells in perivascular regions (*1*), and chemotherapy may promote mobilization of such TIE2^{hi} monocyte progenitors in primary tumors (*8*, *10*). Thus, we focused on and quantified the TIE2^{hi}/VEGF^{hi} macrophage subpopulation using multichannel immunofluorescence (IF) imaging (Fig. 1, G to I, and fig. S2C) (*10*, *14*, *34*). Paclitaxel-treated mice had significantly higher ($P < 0.001$) density of TIE2^{hi}/VEGF^{hi} macrophages compared to the vehicle-treated controls, regardless of whether these were assessed in the entire tissue (fig. S2D) or only in the perivascular niches (Fig. 1G). The proportion of TIE2^{hi}/VEGF^{hi} macrophages among all IBA1$^+$ cells was also increased by paclitaxel treatment (fig. S2, E and F). The significant increase of the perivascular TIE2^{hi}/VEGF^{hi} macrophage subpopulation ($P < 0.0001$) was also demonstrated in the PyMT spontaneous model (Fig. 1G and fig. S2F). Figure 1H illustrates a representative IF image of a TIE2^{hi}/VEGF^{hi} macrophage quantified using CD31, IBA1, VEGF, and TIE2 staining. Figure 1I provides a representative example of VEGF^{hi} and VEGF^{lo} macrophages as seen comparatively in the same field of view, by combining CD31, IBA1, and VEGF staining.

In the PyMT spontaneous model, the total IBA1$^+$ macrophage counts did not correlate with TMEM score (Fig. 1J, left panel), but we did find a correlation ($P < 0.001$) of TMEM with perivascular TIE2^{hi}/VEGF^{hi} macrophages ($R^2 = 0.5$) (Fig. 1J, right panel). In the HT17 xenograft, both total IBA1$^+$ macrophages (Fig. 1K, left panel) and perivascular TIE2^{hi}/VEGF^{hi} macrophages (Fig. 1K, right panel) correlated ($R^2 = 0.65$ and $R^2 = 0.55$, respectively) with TMEM score ($P < 0.001$ in both cases). Both TMEM scores and perivascular TIE2^{hi}/VEGF^{hi} macrophages remained increased upon chemotherapy treatment, even after their values were normalized to microvascular density (fig. S3, A to C). In aggregate, neoadjuvant paclitaxel specifically promotes the assembly of TMEM sites containing TIE2^{hi}/VEGF^{hi} macrophages that are required for TMEM activity in primary breast cancer.

Paclitaxel induces TMEM-dependent vascular permeability in breast tumors

Because chemotherapy treatment may affect blood vessel dynamics by inducing angiogenesis (*9*, *11*–*13*, *35*–*37*), we used IVI (Fig. 2, A and B, and fig. S4A) to investigate whether neoadjuvant paclitaxel induces TMEM-dependent (localized) or TMEM-independent (more universal) blood vessel leakage. Tumors in mice treated with paclitaxel did not demonstrate generalized blood vessel leakage of tetramethylrhodamine (TMR)–conjugated 155-kDa dextran in the extravascular portion of tumors. Instead, they showed localized areas of transient vascular permeability called "bursting" (Fig. 2C and videos S1 and S2), similar to those observed previously in untreated tumors (*1*). In particular, Fig. 2C illustrates a characteristic example of peak bursting activity (still image on the left of Fig. 2C; time lapse in video S1) on a TMEM site, though not all TMEM sites presented with bursting activity (still image on the right of Fig. 2C; time lapse in video S3). All the bursting incidents occurred only at TMEM sites, in close proximity to at least one Dendra2$^+$ tumor cell and one CFP$^+$ macrophage (Fig. 2C, left image). As also reported previously (*1*), we never observed any bursting incidents without juxtaposition to a clearly defined TMEM site. Bursting was documented by the accumulation of dextran-TMR signal over time around an active TMEM site, and no such accumulation was observed away from TMEM (Fig. 2D). The intensity values from all TMEM-mediated bursting incidents observed in paclitaxel-treated mice were averaged and plotted over the entire time of bursting activity (fig. S4B), which confirmed the transient nature of paclitaxel-induced, TMEM-dependent vascular permeability.

To explicitly demonstrate that tumor cell intravasation after paclitaxel treatment is dependent on TMEM-dependent bursting, we measured the tumor cell–specific Dendra2 signal intensity in blood vessel ROIs that were directly juxtaposed to or away from bursting sites (Fig. 2D). The entire time-lapse imaging session of this field can be seen in video S2. Signal intensity of dextran-TMR was also quantified in the corresponding extravascular ROIs to confirm the presence of bursting. We found that cancer cell intravasation in paclitaxel-treated animals occurs during or shortly after the bursting event, specifically at TMEM sites associated with bursting, but never before the bursting event or at TMEM sites without bursting activity (Fig. 2D).

In an independent validation experiment, a group of vehicle- or paclitaxel-treated mice received an intravenous injection of dextran-TMR for 1 hour and was then sacrificed and evaluated for vascular permeability in fixed tumor sections. Multichannel IF staining included endomucin as a blood vessel exclusion mask and an anti-TMR antibody for assessing dextran leakage (fig. S5). A corresponding TMEM IHC staining section was co-aligned to evaluate the presence/absence of

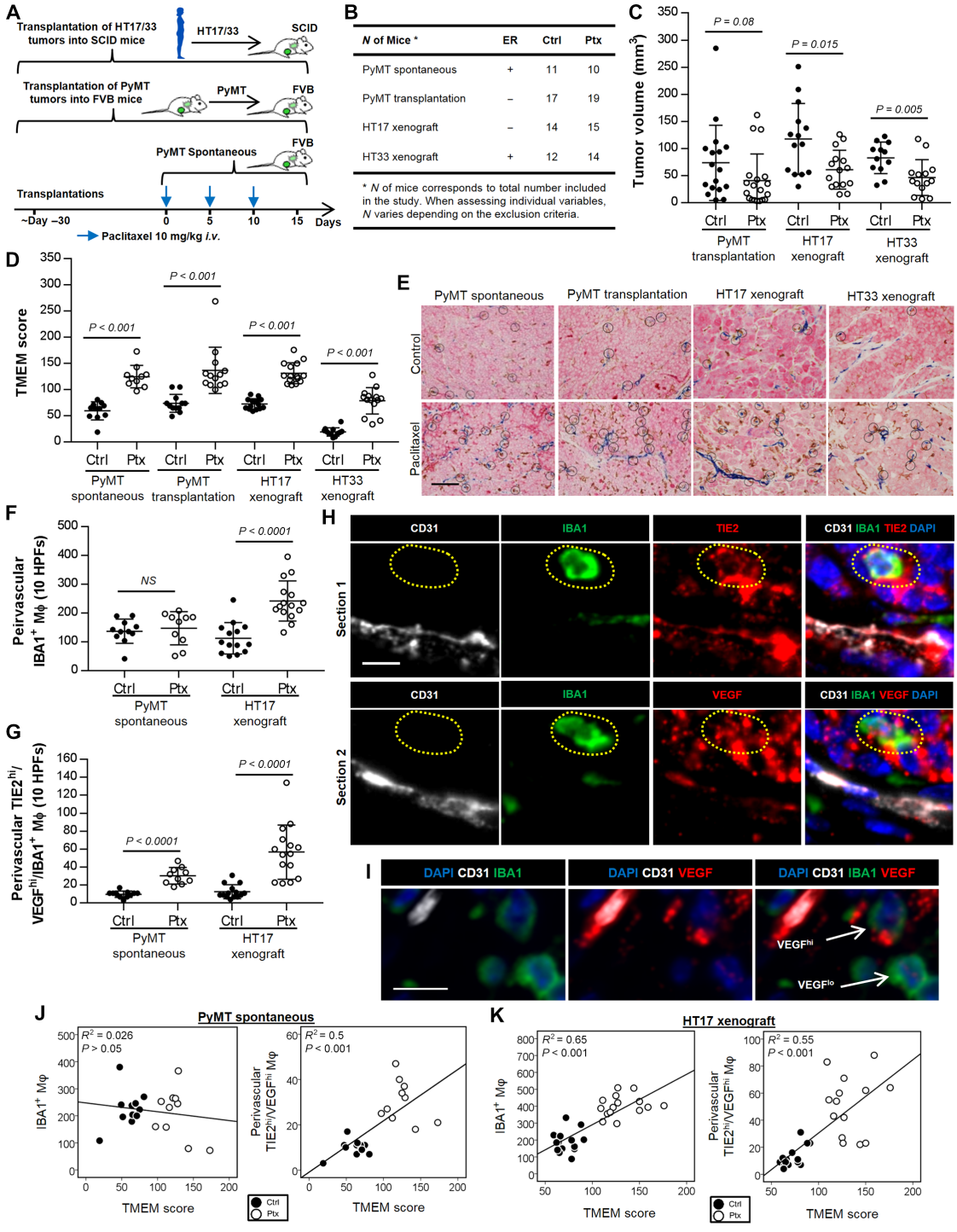

Fig. 1. Paclitaxel delays tumor growth and promotes infiltration of TIE2^{hi}/VEGF^{hi} macrophages and TMEM assembly. (**A**) Experimental design and chemotherapy scheme. i.v., intravenously. (**B**) Mouse models of breast carcinoma, estrogen receptor (ER) status in each model, and cohort sizes. (**C**) Tumor volume quantification on day 15 of the chemotherapy scheme shown in (A). Mann-Whitney *U* test. (**D**) TMEM score, assessed in 10 high-power fields (HPFs) by two pathologists, in mice treated as shown in (A). Mann-Whitney *U* test. (**E**) TMEM identification by triple-stain immunohistochemistry (IHC) and representative images for each mouse model. Scale bar, 50 μm. (**F**) Perivascular IBA1^{+} macrophages (Mφ) in 10 HPFs (absolute counts) in PyMT spontaneous and HT17 xenograft tumors, treated with paclitaxel or vehicle control. Mann-Whitney *U* test. (**G**) Perivascular TIE2^{hi}/VEGF^{hi} macrophages in 10 HPFs (absolute counts) quantified in PyMT spontaneous and HT17 xenograft tumors, treated with paclitaxel or vehicle control. Mann-Whitney *U* test. (**H**) Multichannel IF of IBA1, CD31, TIE2, VEGF, and 4′,6-diamidino-2-phenylindole (DAPI) in two sequential sections of an MMTV-PyMT breast tumor not treated with paclitaxel. Representative VEGF^{hi}/TIE2^{hi} macrophage (also coexpressing IBA1) is encircled with yellow dotted line. Scale bar, 10 μm. (**I**) Multichannel IF of IBA1, CD31, VEGF, and DAPI in an HT17 xenograft tumor, treated with paclitaxel, demonstrating one VEGF^{hi} and one VEGF^{lo} macrophage in a field. Scale bar, 15 μm. (**J** and **K**) Correlations of macrophage infiltration (IBA1^{+} macrophages or VEGF^{hi}/TIE2^{hi} macrophages) with TMEM score in the PyMT spontaneous (J) and HT17 xenograft (K) models. R^2 = Pearson's coefficient of determination; filled circles, control; open circles, paclitaxel.

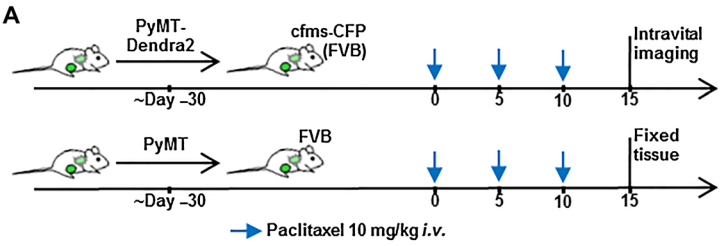

B

Transplantation model *	Purpose	Ctrl	Ptx
PyMT-Dendra2/*cfms*-CFP	Intravital imaging	10	9
PyMT (no-color)	Fixed tissue	5	5

* *N* of mice corresponds to total number included in the study. When assessing individual variables, *N* varies depending on the exclusion criteria.

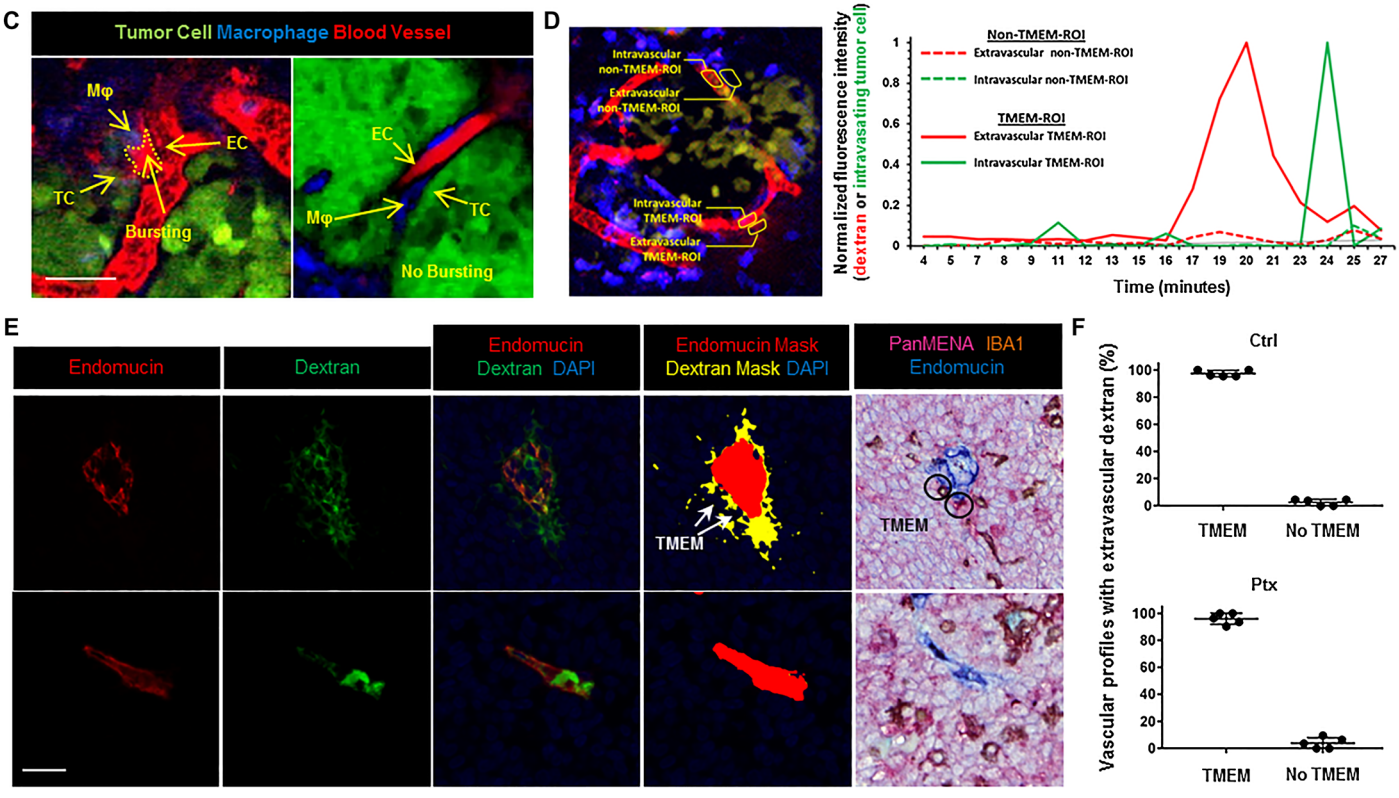

Fig. 2. Paclitaxel induces vascular permeability exclusively at TMEM sites. (**A**) Experimental design and chemotherapy scheme. (**B**) Mouse models of breast carcinoma and cohort sizes. (**C**) Two examples of images taken from IVI of *cfms*-CFP mice grafted with MMTV-PyMT/Dendra2^{+} tumors. Left image: Bursting at TMEM (TMEM activity) identified by the presence of TMR-conjugated 155-kDa dextran in the extravascular space. Outline of the burst indicated by dotted yellow line. Right image: Absence of bursting at TMEM, as a control. Mϕ, macrophage; TC, tumor cell; EC, endothelial cell. Scale bar, 25 μm. (**D**) Left image: Region of interest (ROI) selection for calculation of Dendra2/TMR signal intensity over time. Right graph: The quantification of extravascular dextran (red lines) and Dendra2-labeled intravasating cancer cell (green lines) signal intensity in the selected TMEM-associated (solid lines) or non-TMEM (dotted lines) ROIs from the image shown on the left side. (**E**) Multichannel IF of endomucin (first column), dextran-TMR (second column), their merged image along with DAPI (third column), the corresponding thresholded blood vessel and extravascular dextran masks (fourth column), and the corresponding sequential section of TMEM IHC (fifth column) in MMTV-PyMT mice treated with paclitaxel. Top row: TMEM-associated vascular profile. Bottom row: Vascular profile away from TMEM. Scale bar, 20 μm. (**F**) Percentage of vascular profiles with extravascular dextran that have at least one TMEM site or no TMEM sites associated with them for vehicle-treated (top graph) or paclitaxel-treated (bottom graph) cases.

TMEM in each vascular profile that presented with vascular leakage. Two examples of vascular profiles selected from a paclitaxel-treated mouse are demonstrated in Fig. 2E; the upper row shows a vascular profile with abundant extravascular dextran, which colocalized with two TMEM sites, whereas the lower row shows a vascular profile with absent or minimal extravascular dextran, which colocalized with a blood vessel lacking TMEM (Fig. 2E). For quantification purposes, ~20 to 30 vascular profiles were selected for each mouse, based on tissue size, degree of vascularization, and quality of endomucin staining. In both vehicle-treated and paclitaxel-treated groups, about 96 to 98% of the vascular profiles with extravascular dextran colocalized with at least one TMEM (Fig. 2F).

Paclitaxel increases metastatic dissemination of breast tumors

To assess whether paclitaxel treatment promotes tumor cell dissemination and metastatic incidence, we first used IVI to quantify and compare incidence and frequency of bursting in mice treated with vehicle or paclitaxel (Fig. 3, A to C, and videos S1 and S3). The incidence (at least one bursting event in a ~4.5-hour imaging session) and frequency of bursting were increased in mice treated with paclitaxel, when compared to those treated with vehicle control (Fig. 3, B and C). The same conclusions were reached when frequency of bursting was normalized to the number of TMEM sites, as measured in each field (fig. S6, A and B). Unlike in late-stage tumors, in which TMEM shows spontaneous

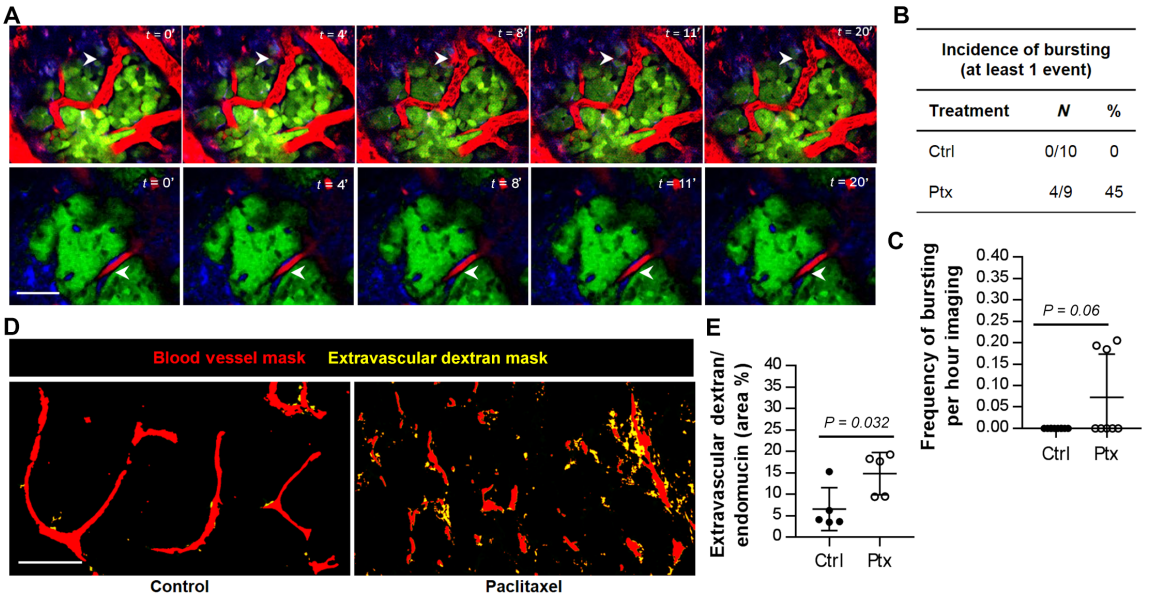

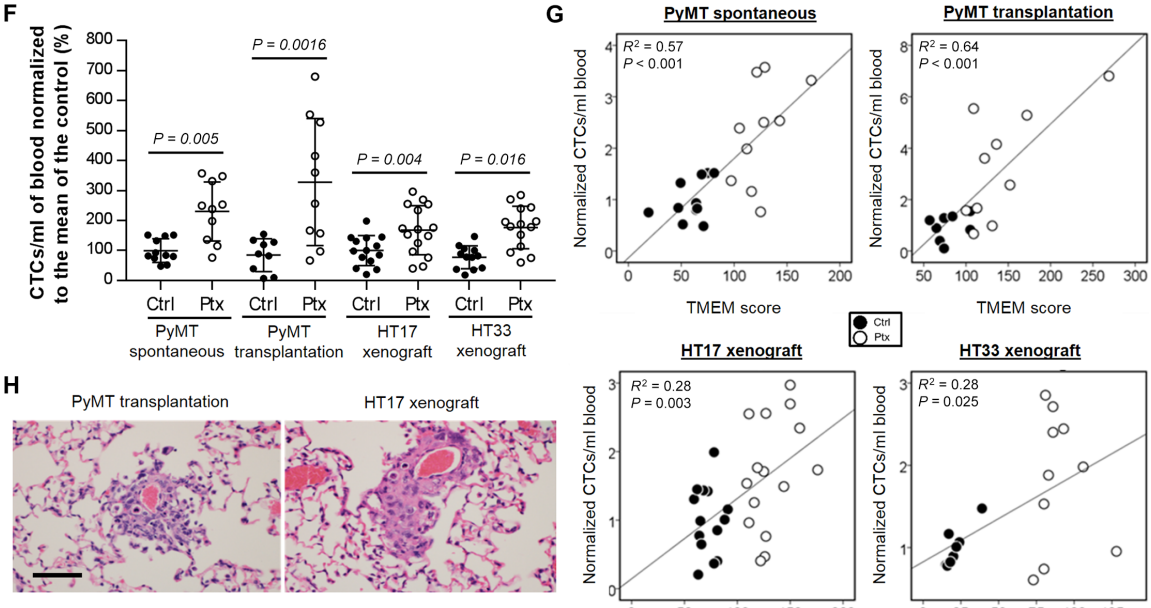

I

Lung metastasis incidence – Histology
Mice with at least 1 focus of >5 tumor cells

Transplant	Ctrl	Ptx	X^2 test
PyMT	2/11 (18.2%)	9/14 (64.3%)	$P < 0.05$
HT17	6/14 (42.9%)	11/15 (73.3%)	$P < 0.1$
HT33	3/12 (25%)	7/10 (70%)	$P < 0.05$

Fisher's exact test used instead, whenever expected value in a cell was <5.

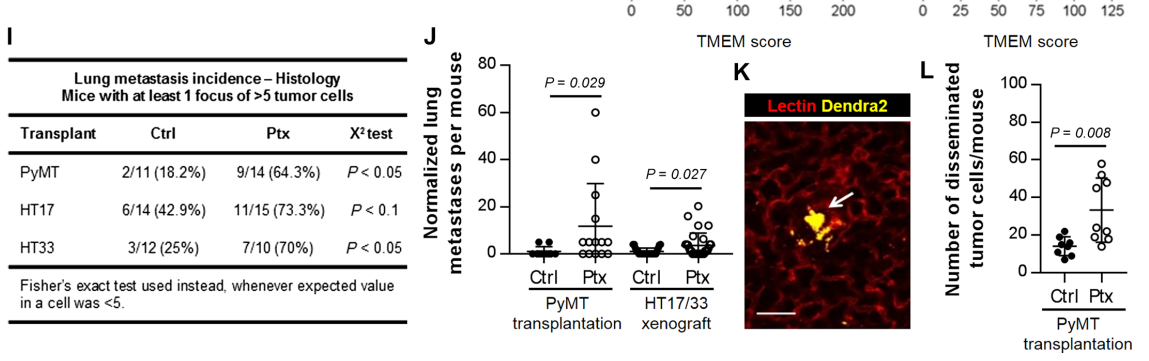

Fig. 3. Paclitaxel promotes TMEM-dependent vascular permeability, cancer cell dissemination, and metastasis in breast cancer. (**A**) Time-lapse images from videos S1 (top row) and S3 (bottom row). Time shown in minutes (t = 0 to 20 min). Top row: Arrowhead follows site of bursting from an active TMEM in a paclitaxel-treated mouse. Bottom row: Arrowhead marks the lack of bursting from an inactive TMEM in a paclitaxel-treated mouse. Scale bar, 50 μm. (**B**) Incidence of bursting (at least one complete event during ~4.5 hours of imaging per mouse) in paclitaxel- and vehicle-treated MMTV-PyMT/Dendra2 *cfms*-CFP mice. (**C**) Frequency of bursting in paclitaxel and control MMTV-PyMT/Dendra2 *cfms*-CFP mice. Mann-Whitney *U* test. (**D**) Representative blood vessel (endomucin) and extravascular dextran masks, as obtained by IF in mice treated with either vehicle or paclitaxel, showing TMEM-associated vascular permeability (yellow area). Scale bar, 100 μm. (**E**) Quantification of extravascular dextran area normalized to blood vessel area in mice treated with either vehicle or paclitaxel shown in (D). Mann-Whitney *U* test. (**F**) CTCs per milliliter of blood collected before sacrifice (day 15). Values normalized to the control group in each case to account for intercohort variability. Mann-Whitney *U* test. (**G**) Correlation between CTCs and TMEM. R^2 = Pearson's coefficient of determination; filled circles, control; open circles, paclitaxel. (**H**) Detection of micrometastatic foci in the lungs of paclitaxel-treated mice. Two cases of histologically detectable metastases in lungs of PyMT transplants and HT17 xenografts, respectively, are shown. Scale bar, 100 μm. (**I**) Incidence of lung metastasis in mice treated with paclitaxel or vehicle control, χ^2 test. (**J**) Quantification of histologically detectable lung metastases in mice treated with paclitaxel or vehicle control. Mann-Whitney *U* test. (**K**) Stereomicroscopy in extracted mouse lung. Blood vessels visualized via tail vein injection of rhodamine-labeled lectin 1 hour before sacrifice, and cancer cells identified through Dendra2 expression (arrow). Mann-Whitney *U* test. Scale bar, 20 μm. (**L**) Quantification of single cancer cell dissemination in lungs of PyMT transplants using fluorescence stereomicroscopy. Mann-Whitney *U* test.

activity as we have already reported (*1*), TMEM-associated bursting is a very rare phenomenon in early carcinoma (Fig. 3C). In addition to IVI, we quantified and compared extravascular dextran area as a percentage normalized to the blood vessel area in fixed tumors of mice treated with either vehicle or paclitaxel, using multichannel IF (Fig. 3, D and E, and fig. S5). Extravascular dextran was about threefold ($P < 0.05$) more abundant in paclitaxel-treated compared to vehicle-treated mice (Fig. 3, D and E).

Having shown that TMEM function is associated with tumor cell intravasation in chemotherapy-treated tumors (Fig. 2D), we then asked whether paclitaxel treatment induces increased metastatic dissemination of breast cancer cells. We found about a twofold increase in circulating tumor cells (CTCs) ($P < 0.05$) after paclitaxel treatment in all experimental models examined (Fig. 3F). TMEM score and CTCs correlated positively in the PyMT spontaneous ($R^2 = 0.57$, $P < 0.001$), PyMT transplantation ($R^2 = 0.63$, $P < 0.001$), as well as the HT17 ($R^2 = 0.28$, $P < 0.05$) and the HT33 ($R^2 = 0.28$, $P < 0.05$) PDX models, though correlations were weaker in the HT17 and HT33 xenografts (Fig. 3G). Because severe combined immunodeficient (SCID) mice used in the PDX models are engineered to lose adaptive immunity but retain innate immunity, it is possible that the weaker correlations were due to a differential degree of immune-mediated rejection of CTCs.

To further determine the effect of paclitaxel on cancer cell dissemination to distant sites, we harvested lungs and evaluated metastatic foci histologically (Fig. 3H and fig. S5). We found an increase in both the metastatic incidence (at least one micrometastatic focus of more than five tumor cells) (Fig. 3I) and the number of cancer cell micrometastases in the lungs of paclitaxel-treated mice (Fig. 3J). In addition, we quantified single-cell dissemination of breast cancer cells in the lungs of FVB recipient mice after syngeneic transplantation of MMTV-PyMT/Dendra2$^+$ tumors using ex vivo microscopy (Fig. 3K and fig. S5) and found about a twofold increase ($P < 0.01$) of single Dendra2$^+$ breast cancer cells in the lungs of paclitaxel-treated mice (Fig. 3L). Overall, these data indicate that, in early-stage breast cancers, chemotherapy increases vascular permeability at TMEM sites, which is accompanied by increased cancer cell dissemination.

Paclitaxel promotes the expression of invasive isoforms of *Mena* in breast tumors

Because our data showed that paclitaxel treatment increases TMEM assembly, as well as TMEM-dependent vascular permeability and metastatic dissemination, we hypothesized that it also increases the proportion of highly migratory cancer cells, which express invasive isoforms of the actin-regulatory protein MENA (*21*, *23*) and are capable of assembling and using TMEM sites to intravasate, a major prerequisite for successful metastatic seeding. To test this hypothesis, we first performed quantitative reverse transcription polymerase chain reaction (qRT-PCR) analysis for total *MENA* (*PanMena*), *Mena11a*, and $Mena^{INV}$ on formalin-fixed paraffin-embedded (FFPE) tumors from the PyMT spontaneous and HT17 xenograft models (fig. S7A). Paclitaxel treatment significantly increased ($P < 0.01$) the expression of *PanMena*, $Mena^{INV}$, and $Mena^{Calc}$, a marker that takes into account the full repertoire of invasive *Mena* isoforms including MENA^{INV} (*38*, *39*), but not that of the antimetastatic *Mena11a* (Fig. 4, A to D), and correlates with distant recurrence in breast cancer patients (*38*, *39*). In addition, both $Mena^{Calc}$ and $Mena^{INV}$ correlated positively with increased TMEM score ($Mena^{INV}$, $P < 0.001$; $Mena^{Calc}$, $P < 0.01$) in both models tested (Fig. 4, E and F), with $Mena^{INV}$ demonstrating higher correlation coefficients than MENA^{Calc}. Paclitaxel-mediated $Mena^{INV}$-increased expression ($P < 0.0001$) and correlation with TMEM score ($P < 0.001$) were also confirmed at the protein level in both the PyMT spontaneous and the HT17 xenograft models (Fig. 4, G to I, and fig. S7, B and C). As shown in the specific MENA^{INV} IF, the pattern of MENA^{INV} expression in PyMT mice was heterogeneous (Fig. 4G and fig. S7C), consistent with previous observations (*40*). We found a positive correlation between TIE2^{hi}/VEGF^{hi} macrophage infiltration and $Mena^{INV}$ expression ($P < 0.001$, $R^2 = 0.68$) (fig. S8A), as well as $Mena^{Calc}$ ($P < 0.05$, $R^2 = 0.24$) (fig. S8B), supporting the evidence that direct contact of tumor cells with macrophages induces $Mena^{INV}$ expression (*27*). In addition, there was an inverse correlation for the antimetastatic *Mena11a* ($P < 0.01$, $R^2 = 0.3$) (fig. S8C).

Paclitaxel promotes breast cancer cell dissemination in a MENA-dependent manner

Animals grafted with MMTV-PyMT MENA-null tumors do not develop CTCs and lung metastases (*28*), indicating that MENA is necessary for tumor cell dissemination. Having shown that paclitaxel increases TMEM assembly (Fig. 1D) and invasive MENA isoform expression (Fig. 4, C, D, G, and H), we next investigated whether paclitaxel-mediated tumor cell dissemination in invasive breast cancer was also MENA-dependent. To test this hypothesis, we orthotopically transplanted MENA$^{-/-}$ or MENA$^{+/+}$ CFP-fluorescent PyMT tumors into wild-type syngeneic hosts to assess tumor cell intravasation and dissemination in the lungs of mice after paclitaxel treatment (Fig. 5, A and B). MENA$^{-/-}$ mice did not express MENA^{INV} protein (fig. S7B). Quantitative assessment of macrophages in the perivascular niches of MENA$^{-/-}$ mice revealed both increased IBA1$^+$ and TIE2^{hi}/VEGF^{hi} IBA1$^+$ macrophage infiltration after paclitaxel treatment (Fig. 5, C to F, and fig. S9, A to C), similar to changes observed in PyMT and HT17 MENA$^{+/+}$ mice after receiving chemotherapy (Fig. 1, F and G). These results indicate that MENA does not interfere with paclitaxel-mediated TIE2^{hi}/VEGF^{hi} macrophage recruitment in the primary breast tumor microenvironment.

Because a MENA-expressing tumor cell constitutes one of the elements of the tripartite TMEM structure, MENA$^{-/-}$ tumors do not assemble TMEM. However, because the perivascular TIE2^{hi}/VEGF^{hi} macrophages could be recruited by paclitaxel treatment even in the MENA$^{-/-}$ tumors (Fig. 5, E and F), we next investigated whether these TIE2^{hi}/VEGF^{hi} macrophages were by themselves sufficient to increase cancer cell dissemination, without the presence of a complete TMEM structure. The absence of the *Mena* gene completely eliminated CTCs ($P < 0.0001$) and the number of single cancer cells disseminating in the lungs ($P < 0.0001$) (Fig. 5, G and H), consistent with previous findings (*28*). This suppression was consistent regardless of vehicle or paclitaxel treatment (Fig. 5, G and H), indicating that the elimination of the *Mena* gene in breast cancers affects cancer cell intravasation and dissemination, although it still permits the paclitaxel-mediated increase of perivascular TIE2^{hi}/VEGF^{hi} macrophages. Thus, paclitaxel treatment in MENA$^{-/-}$ PyMT-CFP transplants failed to boost the number of CTCs in the blood or disseminated cells in the lungs, as seen in the case of MENA$^{+/+}$ mice (Fig. 5, G and H). In summary, these data show that paclitaxel-induced tumor cell dissemination is also dependent on MENA expression, further supporting the essential role of TMEM in paclitaxel-stimulated tumor cell dissemination.

Doxorubicin/cyclophosphamide treatment elicits prometastatic changes similar to paclitaxel in the breast cancer microenvironment

Having shown that paclitaxel induces TMEM- and MENA-mediated prometastatic changes in the primary breast tumor microenvironment

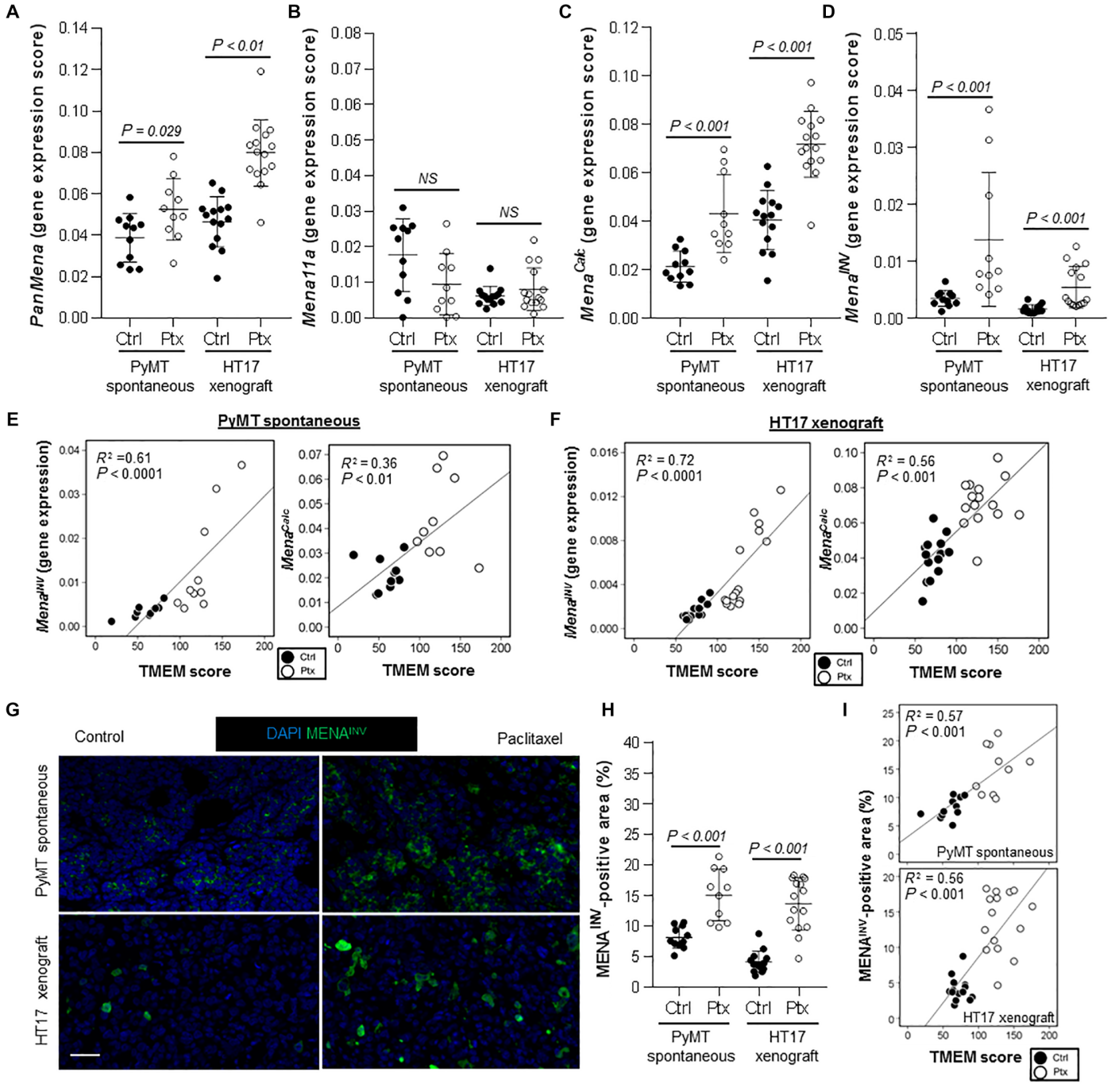

Fig. 4. Paclitaxel promotes the expression of invasive isoforms of MENA in the primary breast cancer microenvironment. (**A** to **D**) Gene expression of MENA or MENA isoforms (real-time RT-PCR) after RNA extraction from FFPE tumors. Gene expression of *Pan-Mena* (A), *Mena11a* (B), *Mena*^{Calc} (C), and *Mena*^{INV} (D) indicated. Mann-Whitney *U* test. NS, not significant. (**E** and **F**) Correlations of *Mena*^{Calc} with TMEM and *Mena*^{INV} gene expression with TMEM in the PyMT spontaneous (E) and HT17 xenograft (F) tumors. R^2 = Pearson's coefficient of determination; filled circles, control; open circles, paclitaxel. (**G**) MENA^{INV} protein expression visualized by MENA^{INV} IF and DAPI in PyMT spontaneous and HT17 xenograft tumors, treated with paclitaxel or vehicle control. Scale bar, 100 μm. (**H**) Quantification of the MENA^{INV}-positive area (%) in tumors shown in (G). Mann-Whitney *U* test. (**I**) Correlation of MENA^{INV}-positive area (%) with TMEM score in the PyMT spontaneous (top plot) and HT17 xenograft (bottom plot) models. R^2 = Pearson's coefficient of determination; filled circles, control; open circles, paclitaxel.

in a wide variety of mouse models, we then examined whether similar effects could be elicited by other chemotherapeutics. We selected the doxorubicin/cyclophosphamide combinatorial chemotherapy because it is a main component of NAC in human breast cancer patients (*41*, *42*). Transgenic MMTV-PyMT mice bearing spontaneous breast tumors received a total of three doses of doxorubicin (5 mg/kg, intravenously) every 5 days and one single dose of cyclophosphamide (120 mg/kg, intraperitoneally) (Fig. 6, A and B). Upon histological examination of the resulting tumors, necrosis and cell death were more evident in the doxorubicin/cyclophosphamide-treated tumors than in vehicle-treated

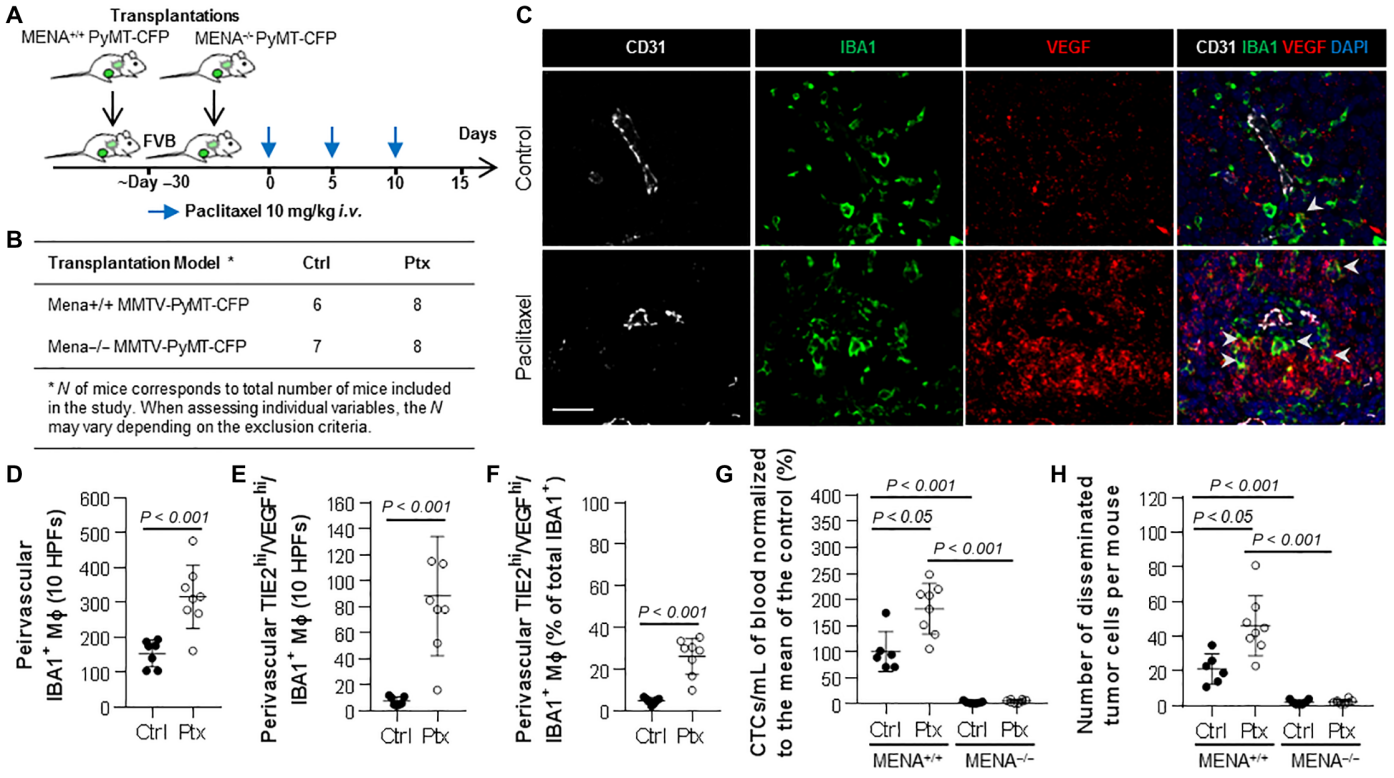

Fig. 5. Paclitaxel promotes breast cancer cell dissemination and metastasis in a MENA-dependent manner. (**A**) Experimental design and chemotherapy scheme. (**B**) Mouse models of breast carcinoma and cohort sizes. (**C**) Multichannel IF of IBA1, CD31, VEGF, and DAPI in MENA$^{-/-}$ MMTV-PyMT-CFP transplanted tumors, treated with either vehicle control (top panel) or paclitaxel (bottom panel). Arrowheads: VEGF^{hi}/IBA1^{+} macrophages. Scale bar, 25 μm. (**D**) Perivascular IBA1^{+} macrophages (Mφ) counted in 10 HPFs (absolute counts) in MENA$^{-/-}$ MMTV-PyMT-CFP transplanted tumors treated with paclitaxel or vehicle control. Mann-Whitney *U* test. (**E** and **F**) Perivascular TIE2^{hi}/VEGF^{hi} macrophages (Mφ) quantified in MENA$^{-/-}$ MMTV-PyMT-CFP transplanted tumors, treated with paclitaxel or vehicle control. Absolute counts (E) or percentages (F) among all perivascular IBA1^{+} macrophages (Mφ). Mann-Whitney *U* test. (**G**) CTCs per milliliter of blood collected from MENA$^{+/+}$ and MENA$^{-/-}$ PyMT-CFP mice. Values normalized to the control group in each case to account for intercohort variability. Mann-Whitney *U* test. (**H**) Quantification of single cancer cell dissemination in the lungs of MENA$^{+/+}$ and MENA$^{-/-}$ PyMT-CFP transplants, using fluorescence stereomicroscopy. Mann-Whitney *U* test.

mice (Fig. 6C). TMEM score was significantly ($P < 0.05$) increased after doxorubicin/cyclophosphamide treatment (Fig. 6, C and D) and was accompanied by a significant ~1.3-fold ($P = 0.027$) increase in the number of CTCs (Fig. 6E), as well as increased numbers of perivascular TIE2^{hi}/VEGF^{hi} macrophages compared to vehicle-treated controls (Fig. 6F). Therefore, the combination of doxorubicin and cyclophosphamide affects TMEM density, TMEM activity, and CTCs in a similar fashion to paclitaxel, further indicating that similar prometastatic effects may be elicited by a variety of NAC regimes.

NAC with paclitaxel induces prometastatic changes in the tumor microenvironment of human breast cancer patients

On the basis of findings shown collectively in Figs. 1 to 6, we then expanded our investigations to human breast cancer patients receiving NAC, containing paclitaxel, doxorubicin, and cyclophosphamide. The change in TMEM density in post-NAC specimens was evaluated in 20 patients with ER^{+}/HER2^{-} disease, who were treated with weekly paclitaxel for up to 12 weeks followed by four cycles of doxorubicin plus cyclophosphamide and had residual disease after NAC [residual cancer burden (RCB) score 2 to 3]. None of the patients received preoperative tamoxifen. When TMEM scores were graphed for each patient individually (Fig. 7A), the following observations were made: (i) Most patients had an increase in TMEM scores after NAC, with a few increasing more than fivefold (patients #3, #11, #15, #19, and #20); (ii) TMEM scores of 50% of patients moved from low/intermediate- into high-risk group (score ≥ 23; red line on the graph) after NAC [TMEM score of 23 was established as the cutoff that separates patients into low/intermediate- and high-risk groups for developing distant metastasis (*5*)]; (iii) TMEM score remained unaltered or even worsened by the end of the treatment in 15% of patients who had high TMEM scores before the NAC (patients #4, #9, and #17); and (iv) there was not a single patient that demonstrated a decrease in TMEM score after NAC. Representative images of TMEM before and after NAC are shown for patients #3 and #7 (Fig. 7B). When analyzed as a cohort, the mean TMEM score was significantly increased (Wilcoxon test; $P < 0.0001$) in post-NAC samples compared to pre-NAC core biopsies (Fig. 7C). These data suggest that NAC may have unwanted long-term consequences in some breast cancer patients.

To further substantiate the translational importance of our preclinical data from PyMT and PDX mice receiving neoadjuvant paclitaxel, we compared MENA^{INV} expression in pre- and post-NAC samples. We observed a significant increase ($P < 0.01$) in MENA^{INV}-positive area between pre-NAC biopsies and post-NAC tumors (Fig. 7, D and E). In addition, we analyzed *MENA^{INV}* expression by qRT-PCR in fine needle aspiration (FNA) biopsies taken before and 1 week after the second dose of weekly paclitaxel in an independent small cohort of patients ($n = 5$).

A

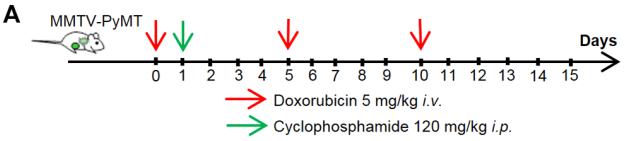

B

Mice *	Ctrl	Doxo/Cyclo
PyMT-spontaneous	9	7

* *N* of mice corresponds to total number of mice included in the study. When assessing individual variables, the *N* may vary depending on the exclusion criteria.

C

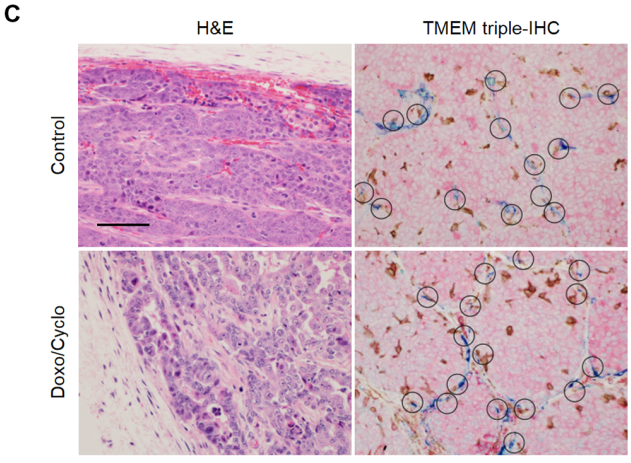

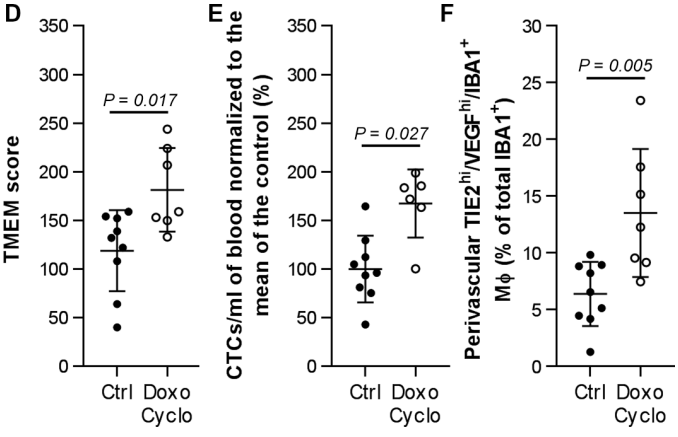

Fig. 6. Nontaxane chemotherapies induce TMEM-dependent prometastatic changes in the breast cancer microenvironment. (**A**) Experimental design and chemotherapy scheme. (**B**) Mouse models of breast carcinoma and cohort sizes. (**C**) Representative histological [hematoxylin and eosin (H&E); left column] and TMEM IHC sections (right column) from MMTV-PyMT mice receiving doxorubicin/cyclophosphamide treatment or vehicle control, as shown in (A). Scale bar, 50 μm. (**D**) TMEM score in MMTV-PyMT mice treated with either vehicle control or doxorubicin/cyclophosphamide. Mann-Whitney *U* test. (**E**) CTCs per milliliter of blood collected before sacrifice (day 15). Values normalized to the control group in each case, to account for intercohort variability. Mann-Whitney *U* test. (**F**) Proportion of perivascular TIE2^{hi}/VEGF^{hi} macrophages among all IBA1^{+} macrophages, quantified in MMTV-PyMT mice treated with either doxorubicin/cyclophosphamide or vehicle control. Mann-Whitney *U* test.

Even at such an early phase of paclitaxel treatment, we were able to observe an increase of *MENA*^{INV} gene expression in four of five breast cancer patients (patients #1 and #3 to #5) (Fig. 7F), suggesting that the TMEM- and MENA-dependent prometastatic changes may have already been initiated in these patients.

Inhibition of the TIE2 receptor reverses the paclitaxel-mediated prometastatic changes

We postulated that selective TIE2 inhibitors could not only be successfully used to counteract the angiogenic potential of NAC-induced endothelial progenitor cell infiltration (*9*, *12*, *13*, *35*, *36*) but also TMEM- and MENA-dependent prometastatic changes, given that TIE2 inhibitors could target TMEM-associated TIE2^{hi}/VEGF^{hi} macrophages.

To address this question, we first investigated the effects of rebastinib, a TIE2 inhibitor, on TMEM assembly, vascular permeability, and CTCs in the PyMT transplantation and HT17 PDX mammary tumor models used in our studies. Animals received NAC with or without rebastinib (Fig. 8, A and B). Treatment with rebastinib alone did not significantly affect the overall TMEM score (Fig. 8, C and D) or the density of perivascular TIE2^{hi}/VEGF^{hi} macrophages (Fig. 8, E and F). However, it significantly ($P < 0.01$) reduced the number of CTCs in both animal models (Fig. 8, G and H), thus impairing hematogenous dissemination, without affecting the assembly of TMEM intravasation sites, indicating inhibition of TMEM activity.

Treatment with paclitaxel alone increased perivascular TIE2^{hi}/VEGF^{hi} macrophages, TMEM assembly, and activity (Fig. 8, C to H), in consistency with Figs. 1 and 3. However, administration of rebastinib in paclitaxel-treated animals decreased the number of perivascular TIE2^{hi}/VEGF^{hi} macrophages (Fig. 8E) and decreased CTCs to the level observed in the control animals (Fig. 8, G and H) without affecting TMEM assembly (Fig. 8, C and D). These data indicate that TIE2 inhibition successfully blocks the function but not the assembly of TMEM sites, which is sufficient to suppress cancer cell dissemination.

We next investigated whether rebastinib-mediated suppression of tumor cell dissemination observed in the paclitaxel-treated mice was due to inhibition of TMEM-associated macrophage function. To address this issue, we used IVI (Fig. 8, A and B) and again found that baseline incidence and frequency of bursting, a TMEM-associated activity, matched to the previously acquired data in the "paclitaxel-only" group (compare Fig. 8, I and J, with Fig. 3, B and C). However, the coadministration of rebastinib in paclitaxel-treated mice completely abolished the incidence and frequency of bursting (Fig. 8, I and J), further suggesting that TIE2 inhibition blocks chemotherapy-driven, TMEM-mediated vascular permeability and cancer cell dissemination.

DISCUSSION

Accumulating evidence indicates that chemotherapy evokes a host repair response, during which bone marrow–derived cells (BMDCs) infiltrate the primary tumor microenvironment and facilitate neoangiogenesis and tumor regrowth (*10*, *11*). Here, we have shown that through such BMDC recruitment, NAC may increase cancer cell dissemination and induce a more aggressive tumor phenotype with increased metastasis. The mechanism involves both the assembly of TMEM sites and the increased MENA^{INV} expression in residual cancer after NAC. These results are consistent with our previous findings that MENA expression is required for TMEM assembly and for cancer cell dissemination through a TMEM MENA^{INV} and TIE2^{hi}/VEGF^{hi} macrophage-dependent mechanism (*1*, *20*, *21*, *29*). Although the effects of taxanes and other chemotherapeutics on neovascularization have been adequately described (*8*, *10*, *12*, *13*, *35*, *43*), our study provides insight into the mechanisms by which paclitaxel and other chemotherapies

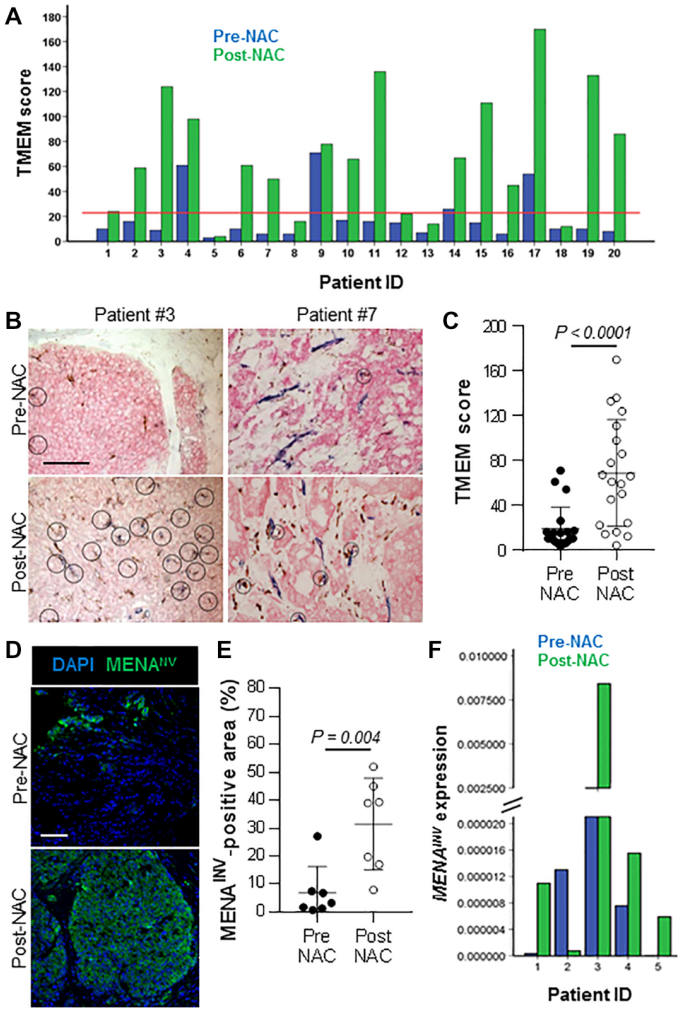

Fig. 7. NAC in breast cancer patients promotes TMEM assembly and increased MENA^{INV} expression. (**A**) Individual TMEM scores of 20 patients before and after receiving NAC, which included weekly paclitaxel (80 mg/m^2 × 12 consecutive weeks) followed sequentially by dose-dense AC chemotherapy [doxorubicin (60 mg/m^2) and cyclophosphamide (600 mg/m^2) every 2 weeks × four cycles, plus pegfilgrastim (6 mg, subcutaneously) on day 2 of each cycle]. The patients did not receive tamoxifen. Red line: TMEM high-risk cutoff point according to (*5*). (**B**) Representative images of TMEM triple-stain IHC in patients #3 and #7 in the pre-NAC core biopsies (upper panels) and post-NAC resected tumors (lower panels). Scale bar, 50 μm. (**C**) Mean TMEM scores in the 20 human breast cancers shown in (A), before and after receiving NAC, Wilcoxon test. (**D**) Representative images of MENA^{INV} protein expression, as visualized by MENA^{INV} IF and DAPI in a patient receiving NAC. Scale bar, 100 μm. (**E**) Quantification of the MENA^{INV}-positive area in pre- and post-NAC patient samples. Assay performed in only seven of the patients shown in (A) because of limited availability of pre-NAC biopsy material for the remaining 13 patients. Mann-Whitney *U* test. (**F**) *MENA^{INV}* gene expression, as assessed by real-time RT-PCR, in FNA biopsies taken from five breast cancer patients before and after 2 weeks of receiving NAC with paclitaxel.

modulate the cancer microenvironment to promote breast cancer cell intravasation and dissemination to distant sites, as well as a TIE2-directed therapeutic approach to counteract paclitaxel-mediated induction of cancer cell dissemination (Fig. 8K). Thus, this work is primarily focused on the chemotherapy effect on cancer cell dissemination via TMEM/MENA-mediated mechanism.

We demonstrated that chemotherapy increases macrophage density in a PDX model but not in spontaneous PyMT. Our findings in the PyMT model are in discrepancy with the Coussens group (*44*). This may be because we worked with 8- to 9-week-old mice bearing early-stage spontaneous carcinomas, whereas the Coussens group worked with 12-week-old mice, which typically have advanced-stage tumors. However, our findings demonstrated that chemotherapy promotes an increase in perivascular TIE2^{hi}/VEGF^{hi} macrophages (Fig. 8K), which is consistent with studies showing that this population associates with sites of (patho)physiological angiogenesis, especially as a host repair mechanism after cytotoxic damage through chemotherapy (*14*, *15*, *45*–*47*). Although it is not clear whether TIE2^{hi}/VEGF^{hi} macrophages belong to the "classically activated" (M1) or "alternatively activated" (M2) group, they are crucial for modulating the tumor microenvironment in response to cytotoxic therapies (*10*, *48*). Our observation that other chemotherapeutics, such as doxorubicin/cyclophosphamide, are capable of perivascular TIE2^{hi}/VEGF^{hi} macrophage recruitment, TMEM assembly, and TMEM-dependent tumor cell intravasation further supports the idea that the mechanism by which chemotherapy induces these prometastatic effects is a generic host repair mechanism in response to extensive tissue damage and not a paclitaxel-specific phenomenon. For instance, TIE2^{+} macrophages also express the chemokine receptor CXCR4, and chemotherapy may increase the expression of the CXCR4 ligand CXCL12 in the primary tumor microenvironment (*10*). Therefore, it is very likely that the prometastatic TIE2^{hi}/VEGF^{hi} macrophages are recruited through a distinct chemotactic axis in chemotherapy-treated individuals.

In addition, increased macrophage infiltration into tumors upon paclitaxel treatment increases the contact between tumor cells and macrophages, which is known to stimulate the expression of MENA^{INV} via NOTCH pathway activation, resulting in increased MENA^{INV} and TMEM-dependent intravasation (*27*). These observations suggest that paclitaxel treatment may have induced MENA^{INV} and MENA^{Calc} expression due to chemotherapy-driven macrophage infiltration, resulting in increased TMEM assembly and function as described here (Fig. 8K). This may be an active process and not simply the result of selective survival of MENA-expressing tumor cells during paclitaxel treatment (*49*). Otherwise, our data are in agreement with findings from Oudin *et al.* (*49*), who showed increased MENA and MENA^{INV} expression in paclitaxel-treated compared to control MDA-MB-231 xenografts.

The observed increase in disseminating tumor cells upon chemotherapy treatment as a direct consequence of macrophage contact–induced MENA^{INV} overexpression is supported by two key findings reported here. First, MENA^{INV} and MENA^{Calc} expression correlated especially well with TIE2^{hi} macrophages, consistent with earlier studies in humans and in mice (*18*, *20*, *29*). Second, the absence of all MENA isoforms completely abolished cancer cell dissemination and distant metastasis in vivo, regardless of whether those mice received paclitaxel or not and without affecting TIE2^{hi}/VEGF^{hi} macrophage recruitment, indicating that MENA expression is an essential prerequisite for paclitaxel-induced breast cancer cell transendothelial migration in vivo.

Our study indicates that the TMEM score and MENA^{INV} increase in breast cancer samples from patients treated with NAC including doxorubicin, cyclophosphamide, and paclitaxel, suggesting that TMEM score and MENA^{INV} might be used in predicting development of prometastatic changes in primary tumor microenvironment in response to NAC. This is important because many breast cancer patients are treated with NAC, which typically lasts about 6 months, and currently, there

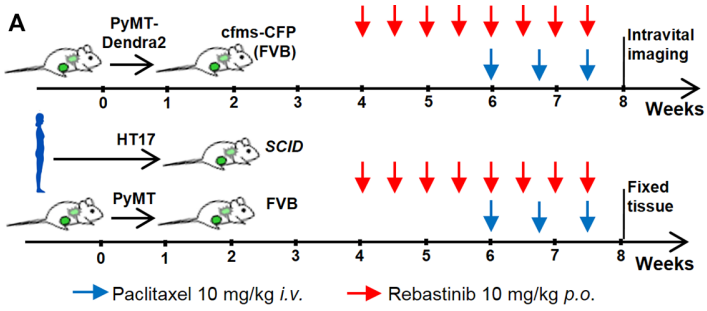

B

Mice *	Purpose	Ctrl	Reb	Ptx	Ptx+Reb
PyMT-Dendra2/*cfms*-CFP	IVI	–	–	12	13
PyMT transplantation	Fixed	7	7	7	8
HT17 xenograft	Fixed	10	12	11	12

* *N* of mice corresponds to total number of mice included in the study. When assessing individual variables, the *N* may vary depending on the exclusion criteria.

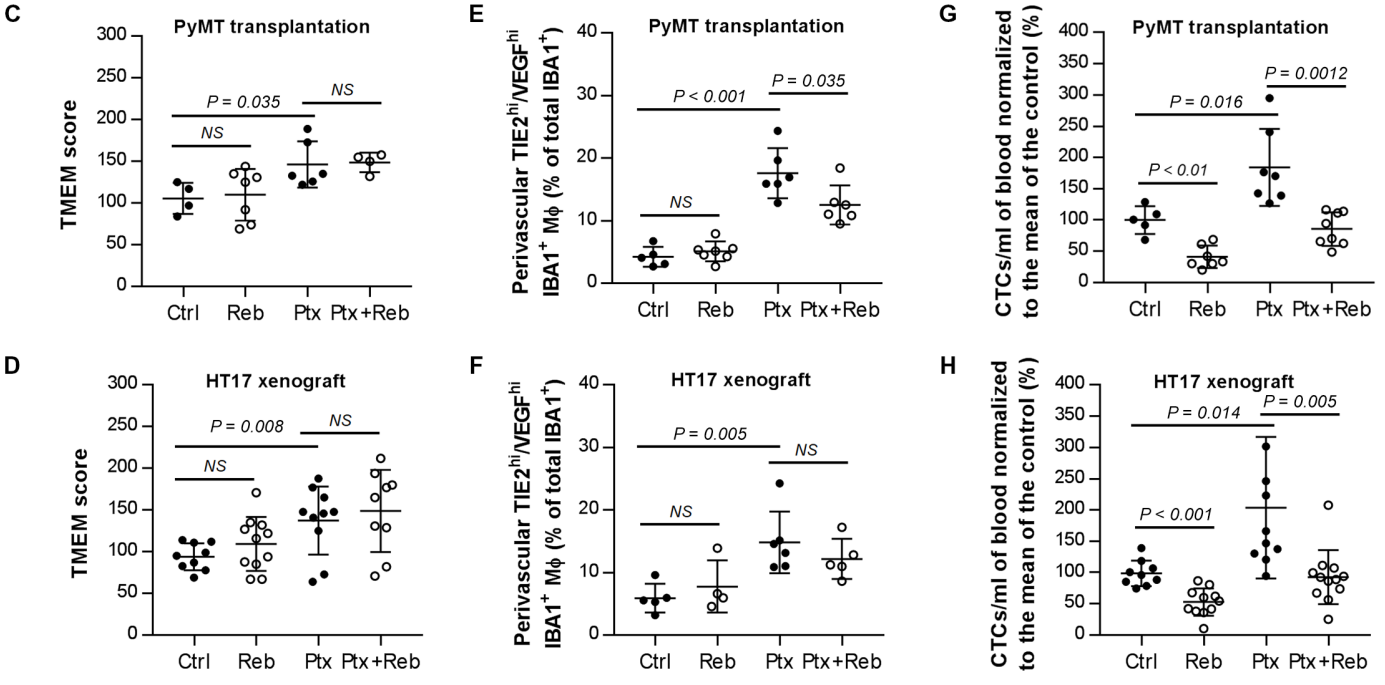

I

Incidence of bursting (at least 1 event)		
Treatment	***N***	**%**
Ptx	5/12	42
Ptx+Reb	0/13	0

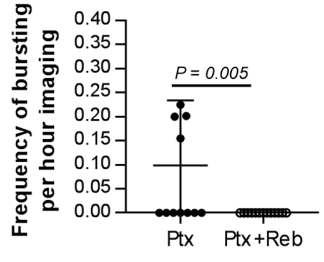

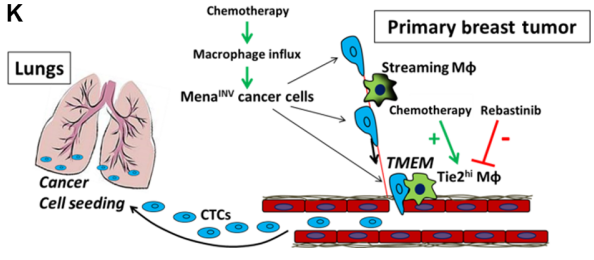

Fig. 8. TIE2 inhibitor rebastinib eliminates the prometastatic effects of paclitaxel. (**A**) Experimental design and chemotherapy scheme. (**B**) Mouse models of breast carcinoma and cohort sizes. (**C** and **D**) TMEM scores in the PyMT transplantation model (C) and the HT17 xenograft model (D), treated with vehicle control, rebastinib, paclitaxel, or a combination of rebastinib with paclitaxel. Mann-Whitney *U* test. (**E** and **F**) Perivascular TIE2^{hi}/VEGF^{hi} macrophages quantified in 10 HPFs in the PyMT transplantation model (E) or in the HT17 xenograft model (F), treated with vehicle control rebastinib, paclitaxel, or a combination of rebastinib with paclitaxel. Mann-Whitney *U* test. (**G** and **H**) CTCs per milliliter of blood collected before sacrifice (day 15) of mice [PyMT transplantation (G); HT17 xenograft (H)]. Values normalized to the control group in each case to account for intercohort variability. Mann-Whitney *U* test. (**I**) Incidence of bursting (at least one complete event during 4.5 hours of imaging per mouse) in paclitaxel-treated MMTV-PyMT/Dendra2 *cfms*-CFP mice that either received or did not receive rebastinib. (**J**) Frequency of bursting in paclitaxel-treated MMTV-PyMT/Dendra2 *cfms*-CFP mice that either received or did not receive rebastinib. Mann-Whitney *U* test. (**K**) Proposed model of chemotherapy-induced prometastatic changes and cancer cell dissemination. Chemotherapy treatment increases the density of TIE2^{hi}/VEGF^{hi} macrophages within the primary tumor. In addition to inducing angiogenesis, these macrophages assemble active TMEM structures. Chemotherapy treatment also increases expression of the actin-regulatory protein MENA^{INV} isoform in tumor cells due to their contact with infiltrating macrophages, which makes these cancer cells highly migratory and invasive. Upon arriving at the blood vessels, some of the MENA^{INV}-expressing cancer cells assemble active TMEM sites, which other MENA^{INV}-expressing cells then use to intravasate. Together, chemotherapy-mediated MENA^{INV} overexpression and TMEM assembly in breast cancer contribute to TMEM-dependent cancer cell dissemination and distant metastasis. Targeting the function of TMEM-associated macrophage subpopulation by a TIE2 inhibitor counteracts TMEM-mediated cancer cell dissemination induced by chemotherapy treatment.

are no markers that predict response to NAC (*43*). Our data indicate that in patients who have RCB post-NAC, such as those with ER^+ disease, NAC could induce metastases via TMEM, despite inducing partial tumor regression. In particular, only 16.5% of patients with $ER^+/HER2^-$ disease achieve pathologic complete response (pCR) with NAC, indicating that our findings may apply to the majority of patients, that is, those who do not achieve pCR (*50*). Although addition of paclitaxel to NAC increases the percentage of patients with pCR, it does not improve the overall survival (*6*, *7*), suggesting that some patients do not draw long-term benefit from NAC. Because we showed that after only two doses of chemotherapy, $MENA^{INV}$ increases in some patients, we speculate that MENA isoform expression status in FNA biopsy after the first 2 weeks of chemotherapy could predict which patients would receive full benefit from NAC and in which continuation of NAC would be harmful. For example, an approach could be developed to routinely assess the expression of $MENA^{INV}$ in FNA samples after the second chemotherapeutic dose. If the invasive isoforms of MENA do not increase, then the chemotherapy could be continued to its completion. Conversely, if there is an increase in the invasive MENA isoform, then the chemotherapy could be discontinued and these patients could be treated with surgery first, followed by chemotherapy. However, the effectiveness of such an approach would need to be investigated in future studies.

Our cohort of 20 patients with ER^+ disease had only 5 years of follow-up time, which is not sufficient to reliably analyze distant recurrence in this breast cancer subtype because ER^+ disease often recurs 10 or more years after the initial diagnosis (*51*). However, two retrospective-prospective analyses of human breast cancer samples indicate that increased TMEM score is associated with metastatic outcome in patients (*3*, *5*). These studies imply that with the proper follow-up time, the increase in TMEM score upon chemotherapy should translate into distant recurrence in some of the patients. A follow-up study is needed to determine whether patients with an increase in TMEM score upon NAC develop distant recurrence more often than those without an increase in TMEM score. In addition, as discussed above, it is necessary to determine whether we can predict which patients are likely to respond to NAC by assessing $MENA^{INV}$ so that the treatment can be adjusted accordingly.

To accurately reflect clinically relevant scenarios, we primarily used early-stage PyMT tumors in our study. As reported by American Cancer Society in *Breast Cancer Facts & Figures 2015-2016*,the incidence rate is the highest for tumors <2 cm (70 per 100,000), followed by tumors 2 to 4.9 cm (35 per 100,000) (*32*). Tumors >5 cm had an incidence rate of only 10 per 100,000. Likewise, the incidence rate for localized (40 to 90 per 100,000) and regional (25 to 40 per 100,000) disease far exceeds the incidence rate for distant (5 to 11 per 100,000) disease (*32*). In addition, by selecting early-stage PyMT tumors, we have avoided measuring potentially TMEM-independent mechanisms of cancer cell dissemination that could result from an open circulation effect, such as upon destruction of the vasculature in advanced-stage necrotic lesions.

Our finding that paclitaxel induces an increase in CTCs is consistent with recently reported data from patient studies focused on the effect of chemotherapy on CTCs. Although CTC count measured by U.S. Food and Drug Administration–approved CellSearch System is a strong prognostic factor in both primary and metastatic breast cancer, there is no conclusive evidence in the literature that chemotherapy significantly reduces CTCs (*52*). On the contrary, several reports indicate that CTC counts in post-chemotherapy blood samples increase in some patients and decrease in others, do not correlate with pCR, and correlate with distant metastasis–free survival (*53*, *54*). Moreover, when CTC search included cells with epithelial-mesenchymal transition marker expression, 21% of patients showed increased CTC counts after NAC, whereas 15% showed a decrease in CTCs counts after NAC (*54*). Thus, our data indicating that NAC may be increasing CTCs in some patients are consistent with current literature.

One limitation of this study is that it does not fully address the development of clinically detectable metastases, which involves other processes such as release from dormancy and tumor growth in addition to cancer cell dissemination. Another limitation is that, due to a long time between the diagnosis and the relapse in ER^+ disease, this study could not provide evidence that increased TMEM and $MENA^{INV}$ in post-NAC patient samples correlate with metastatic outcome.

Because metastatic disease is the major cause of cancer-related mortality and is currently incurable, it is critical that we develop strategies to prevent progression of cancer to the metastatic stage and to prevent further spread from already existing metastatic foci. Therefore, our finding that chemotherapy, when given in the setting of clinically active disease, may promote cancer cell dissemination is of major concern. However, our data indicate that strategies can be developed to prevent chemotherapy-induced TMEM/MENA-mediated cancer cell dissemination and subsequent metastasis. This can be done either by discontinuing NAC in patients whose tumors show NAC-induced prometastatic changes or by combining NAC with agents that block TMEM/MENA-mediated cancer cell dissemination, such as selective TIE2 inhibitors, which would be useful not only in NAC treatment of localized breast cancer but also in treatment of metastatic breast cancer.

MATERIALS AND METHODS

Study design

The primary objective of this study was to examine the prometastatic effects of NAC in mouse models of breast cancer, breast cancer PDXs, and human patients. Mice were randomly allocated to two treatment groups: vehicle-treated and chemotherapy-treated. Two chemotherapy schemes were performed: paclitaxel or doxorubicin/cyclophosphamide. After the termination of treatment, mice were either subjected to IVI to assess the effect of chemotherapy on vascular permeability (bursting) or sacrificed and assessed for $TIE2^{hi}/VEGF^{hi}$ macrophages, TMEM assembly, TMEM-dependent vascular permeability, CTCs, metastatic dissemination in the lungs, and gene and protein expression of the invasive MENA isoform $MENA^{INV}$. The secondary objective was to examine whether the TIE2 inhibitor, rebastinib, is capable of suppressing the chemotherapy-mediated prometastatic effects described in the first part of the study in the same mouse models of breast cancer. All mice received NAC with paclitaxel and were randomly allocated to two groups: vehicle- or rebastinib-treated. After the termination of treatment, mice were either subjected to IVI or sacrificed to assess $TIE2^{hi}/VEGF^{hi}$ macrophages, TMEM assembly, and CTCs.

Statistical analysis

GraphPad Prism 6 software was used for graph/plot generation and statistical hypothesis testing. Continuous variables (tumor volume, TMEM score, CTCs per milliliter of blood, macrophage count, and gene and protein expression values) are presented as dot plots with means and SD. Comparisons between two independent samples were performed using two-tailed Mann-Whitney *U* test, and matched-sample comparisons were performed using the Wilcoxon test. Correlations

were analyzed using Pearson's correlation and coefficient of determination (R^2), and the data are presented as scatterplots with fit lines and corresponding P values. To investigate for differences in binary outcomes (incidence of metastasis) between two groups, cross-tabulation and χ^2 tests were performed. In all graphs, P values of <0.1 are reported; however, only P values of <0.05 are described as statistically significant.

Sample size calculations were performed using the following parameters: significance level (adjusted for sidedness) of 0.025, probability of type II error of 0.2 (statistical power of 0.8), and expected difference in means equal to 1.2 SD units, based on the assumption that the SD of the response variable was 1 unit. A total of 22 animals (11 animals per group) was calculated to enter all two-treatment parallel studies.

The following animals were removed from the study: mice whose tumors were necrotic or cystic; mice with inadequate tumor tissue to perform TMEM counting, IHC/IF, or RNA extraction; mice with less than 0.5 ml of blood collected through heart puncture for the CTC assay; and mice that were either obese (>33 g) or emaciated (<17 g). Accordingly, in each individual figure panel, the number of mice may have been reduced up to 25% from the original cohort sizes depicted in the corresponding figures (Figs. 1B, 2B, 5B, 6B, and 8B).

Transgenic MMTV-PyMT animals, as well as animals transplanted with syngeneic or patient-derived tumors, were housed in cages of five animals, as per the regulations of the Albert Einstein College of Medicine Animal Care and Use Committee. Once they reached the criteria for inclusion into the experimental pipeline (tumor diameter of ~2 to 3 mm), animals were randomly assigned to the chemotherapy-treated, rebastinib-treated, or vehicle-treated groups.

All pathologists involved in TMEM scoring were blinded to the group allocation (fig. S10), as were the scientists performing IVI, CTC scoring, IF/IHC, and qRT-PCR analyses in mouse and human samples. However, pre-NAC biopsies in human patients are microscopically easy to differentiate from resected whole tumor tissues, and as such, blinding was not possible for TMEM assessment in human breast cancer patients receiving NAC.

SUPPLEMENTARY MATERIALS

www.sciencetranslationalmedicine.org/cgi/content/full/9/397/eaan0026/DC1
Materials and Methods
Fig. S1. Histological sections of control and paclitaxel-treated mice.
Fig. S2. Macrophage population dynamics in control and paclitaxel-treated mice.
Fig. S3. Microvascular density in control and paclitaxel-treated mice.
Fig. S4. IVI and extravascular dextran intensity analysis.
Fig. S5. Experimental design of in vivo metastasis dissemination assays.
Fig. S6. Frequency of bursting normalized to TMEM sites.
Fig. S7. MENA^{INV} expression at the gene and protein levels.
Fig. S8. The association of *Mena* isoform expression with TIE2^{hi}/VEGF^{hi} macrophages.
Fig. S9. Macrophage population dynamics after paclitaxel treatment in MENA$^{-/-}$ mice.
Fig. S10. Correlation of TMEM scoring between pathologists.
Table S1. Forward and reverse primer sequences used to identify transmission of the disrupted *Mena* allele in MENA$^{-/-}$ mice.
Video S1. Bursting close to a TMEM site of a paclitaxel-treated mouse.
Video S2. Bursting close to a TMEM site of a second paclitaxel-treated mouse.
Video S3. Absence of bursting in the vasculature of a paclitaxel-treated mouse.
References (*55*–*65*)

REFERENCES AND NOTES

1. A. S. Harney, E. N. Arwert, D. Entenberg, Y. Wang, P. Guo, B.-Z. Qian, M. H. Oktay, J. W. Pollard, J. G. Jones, J. S. Condeelis, Real-time imaging reveals local, transient vascular permeability, and tumor cell intravasation stimulated by TIE2^{hi} macrophage–derived VEGFA. *Cancer Discov.* **5**, 932–943 (2015).
2. G. S. Karagiannis, S. Goswami, J. G. Jones, M. H. Oktay, J. S. Condeelis, Signatures of breast cancer metastasis at a glance. *J. Cell Sci.* **129**, 1751–1758 (2016).
3. B. D. Robinson, G. L. Sica, Y.-F. Liu, T. E. Rohan, F. B. Gertler, J. S. Condeelis, J. G. Jones, Tumor microenvironment of metastasis in human breast carcinoma: A potential prognostic marker linked to hematogenous dissemination. *Clin. Cancer Res.* **15**, 2433–2441 (2009).
4. M. H. Oktay, F. B. Gertler, Y.-F. Liu, T. E. Rohan, J. S. Condeelis, J. G. Jones, Correlated immunohistochemical and cytological assays for the prediction of hematogenous dissemination of breast cancer. *J. Histochem. Cytochem.* **60**, 168–173 (2012).
5. T. E. Rohan, X. Xue, H.-M. Lin, T. M. D'Alfonso, P. S. Ginter, M. H. Oktay, B. D. Robinson, M. Ginsberg, F. B. Gertler, A. G. Glass, J. A. Sparano, J. S. Condeelis, J. G. Jones, Tumor microenvironment of metastasis and risk of distant metastasis of breast cancer. *J. Natl. Cancer Inst.* **106**, dju136 (2014).
6. P. Rastogi, S. J. Anderson, H. D. Bear, C. E. Geyer, M. S. Kahlenberg, A. Robidoux, R. G. Margolese, J. L. Hoehn, V. G. Vogel, S. R. Dakhil, D. Tamkus, K. M. King, E. R. Pajon, M. J. Wright, J. Robert, S. Paik, E. P. Mamounas, N. Wolmark, Preoperative chemotherapy: Updates of National Surgical Adjuvant Breast and Bowel Project Protocols B-18 and B-27. *J. Clin. Oncol.* **26**, 778–785 (2008).
7. L. Gianni, J. Baselga, W. Eiermann, V. G. Porta, V. Semiglazov, A. Lluch, M. Zambetti, D. Sabadell, G. Raab, A. L. Cussac, A. Bozhok, A. Martinez-Agulló, M. Greco, M. Byakhov, J. J. L. Lopez, M. Mansutti, P. Valagussa, G. Bonadonna, Phase III trial evaluating the addition of paclitaxel to doxorubicin followed by cyclophosphamide, methotrexate, and fluorouracil, as adjuvant or primary systemic therapy: European Cooperative Trial in Operable Breast Cancer. *J. Clin. Oncol.* **27**, 2474–2481 (2009).
8. L. G. M. Daenen, J. M. Houthuijzen, G. A. Cirkel, J. M. L. Roodhart, Y. Shaked, E. E. Voest, Treatment-induced host-mediated mechanisms reducing the efficacy of antitumor therapies. *Oncogene* **33**, 1341–1347 (2014).
9. M. De Palma, C. E. Lewis, Macrophage regulation of tumor responses to anticancer therapies. *Cancer Cell* **23**, 277–286 (2013).
10. R. Hughes, B.-Z. Qian, C. Rowan, M. Muthana, I. Keklikoglou, O. C. Olson, S. Tazzyman, S. Danson, C. Addison, M. Clemons, A. M. Gonzalez-Angulo, J. A. Joyce, M. De Palma, J. W. Pollard, C. E. Lewis, Perivascular M2 macrophages stimulate tumor relapse after chemotherapy. *Cancer Res.* **75**, 3479–3491 (2015).
11. J. M. L. Roodhart, H. He, L. G. M. Daenen, A. Monvoisin, C. L. Barber, M. van Amersfoort, J. J. Hofmann, F. Radtke, T. F. Lane, E. E. Voest, M. L. Iruela-Arispe, Notch1 regulates angio-supportive bone marrow–derived cells in mice: Relevance to chemoresistance. *Blood* **122**, 143–153 (2013).
12. Y. Shaked, A. Ciarrocchi, M. Franco, C. R. Lee, S. Man, A. M. Cheung, D. J. Hicklin, D. Chaplin, F. S. Foster, R. Benezra, R. S. Kerbel, Therapy-induced acute recruitment of circulating endothelial progenitor cells to tumors. *Science* **313**, 1785–1787 (2006).
13. Y. Shaked, E. Henke, J. M. L. Roodhart, P. Mancuso, M. H. G. Langenberg, M. Colleoni, L. G. Daenen, S. Man, P. Xu, U. Emmenegger, T. Tang, Z. Zhu, L. Witte, R. M. Strieter, F. Bertolini, E. E. Voest, R. Benezra, R. S. Kerbel, Rapid chemotherapy-induced acute endothelial progenitor cell mobilization: Implications for antiangiogenic drugs as chemosensitizing agents. *Cancer Cell* **14**, 263–273 (2008).
14. M. De Palma, M. A. Venneri, R. Galli, L. Sergi Sergi, L. S. Politi, M. Sampaolesi, L. Naldini, Tie2 identifies a hematopoietic lineage of proangiogenic monocytes required for tumor vessel formation and a mesenchymal population of pericyte progenitors. *Cancer Cell* **8**, 211–226 (2005).
15. M. De Palma, M. A. Venneri, C. Roca, L. Naldini, Targeting exogenous genes to tumor angiogenesis by transplantation of genetically modified hematopoietic stem cells. *Nat. Med.* **9**, 789–795 (2003).
16. A. Dovas, A. Patsialou, A. S. Harney, J. Condeelis, D. Cox, Imaging interactions between macrophages and tumour cells that are involved in metastasis in vivo and in vitro. *J. Microsc.* **251**, 261–269 (2013).
17. A. Patsialou, J. J. Bravo-Cordero, Y. Wang, D. Entenberg, H. Liu, M. Clarke, J. S. Condeelis, Intravital multiphoton imaging reveals multicellular streaming as a crucial component of in vivo cell migration in human breast tumors. *Intravital* **2**, e25294 (2013).
18. E. T. Roussos, J. S. Condeelis, A. Patsialou, Chemotaxis in cancer. *Nat. Rev. Cancer* **11**, 573–587 (2011).
19. S. Goswami, U. Philippar, D. Sun, A. Patsialou, J. Avraham, W. Wang, F. Di Modugno, P. Nistico, F. B. Gertler, J. S. Condeelis, Identification of invasion specific splice variants of the cytoskeletal protein Mena present in mammary tumor cells during invasion in vivo. *Clin. Exp. Metastasis* **26**, 153–159 (2009).
20. E. T. Roussos, S. Goswami, M. Balsamo, Y. Wang, R. Stobezki, E. Adler, B. D. Robinson, J. G. Jones, F. B. Gertler, J. S. Condeelis, M. H. Oktay, Mena invasive (Mena^{INV}) and Mena11a isoforms play distinct roles in breast cancer cell cohesion and association with TMEM. *Clin. Exp. Metastasis* **28**, 515–527 (2011).
21. E. T. Roussos, M. Balsamo, S. K. Alford, J. B. Wyckoff, B. Gligorijevic, Y. Wang, M. Pozzuto, R. Stobezki, S. Goswami, J. E. Segall, D. A. Lauffenburger, A. R. Bresnick, F. B. Gertler, J. S. Condeelis, Mena invasive (Mena^{INV}) promotes multicellular streaming motility and transendothelial migration in a mouse model of breast cancer. *J. Cell Sci.* **124**, 2120–2131 (2011).

22. J. Wyckoff, W. Wang, E. Y. Lin, Y. Wang, F. Pixley, E. R. Stanley, T. Graf, J. W. Pollard, J. Segall, J. Condeelis, A paracrine loop between tumor cells and macrophages is required for tumor cell migration in mammary tumors. *Cancer Res.* **64**, 7022–7029 (2004).
23. U. Philippar, E. T. Roussos, M. Oser, H. Yamaguchi, H.-D. Kim, S. Giampieri, Y. Wang, S. Goswami, J. B. Wyckoff, D. A. Lauffenburger, E. Sahai, J. S. Condeelis, F. B. Gertler, A Mena invasion isoform potentiates EGF-induced carcinoma cell invasion and metastasis. *Dev. Cell* **15**, 813–828 (2008).
24. A. Patsialou, J. Wyckoff, Y. Wang, S. Goswami, E. R. Stanley, J. S. Condeelis, Invasion of human breast cancer cells in vivo requires both paracrine and autocrine loops involving the colony-stimulating factor-1 receptor. *Cancer Res.* **69**, 9498–9506 (2009).
25. S. Goswami, E. Sahai, J. B. Wyckoff, M. Cammer, D. Cox, F. J. Pixley, E. R. Stanley, J. E. Segall, J. S. Condeelis, Macrophages promote the invasion of breast carcinoma cells via a colony-stimulating factor-1/epidermal growth factor paracrine loop. *Cancer Res.* **65**, 5278–5283 (2005).
26. E. Leung, A. Xue, Y. Wang, P. Rougerie, V. P. Sharma, R. Eddy, D. Cox, J. Condeelis, Blood vessel endothelium-directed tumor cell streaming in breast tumors requires the HGF/C-Met signaling pathway. *Oncogene* **36**, 2680–2692 (2017).
27. J. Pignatelli, J. J. Bravo-Cordero, M. Roh-Johnson, S. J. Gandhi, Y. Wang, X. Chen, R. J. Eddy, A. Xue, R. H. Singer, L. Hodgson, M. H. Oktay, J. S. Condeelis, Macrophage-dependent tumor cell transendothelial migration is mediated by Notch1/Mena^{INV}-initiated invadopodium formation. *Sci. Rep.* **6**, 37874 (2016).
28. E. T. Roussos, Y. Wang, J. B. Wyckoff, R. S. Sellers, W. Wang, J. Li, J. W. Pollard, F. B. Gertler, J. S. Condeelis, Mena deficiency delays tumor progression and decreases metastasis in polyoma middle-T transgenic mouse mammary tumors. *Breast Cancer Res.* **12**, R101 (2010).
29. J. Pignatelli, S. Goswami, J. G. Jones, T. E. Rohan, E. Pieri, X. Chen, E. Adler, D. Cox, S. Maleki, A. Bresnick, F. B. Gertler, J. S. Condeelis, M. H. Oktay, Invasive breast carcinoma cells from patients exhibit Mena^{INV}- and macrophage-dependent transendothelial migration. *Sci. Signal.* **7**, ra112 (2014).
30. L. Chen, J. Li, F. Wang, C. Dai, F. Wu, X. Liu, T. Li, R. Glauben, Y. Zhang, G. Nie, Y. He, Z. Qin, Tie2 expression on macrophages is required for blood vessel reconstruction and tumor relapse after chemotherapy. *Cancer Res.* **76**, 6828–6838 (2016).
31. A. Patsialou, Y. Wang, J. Lin, K. Whitney, S. Goswami, P. A. Kenny, J. S. Condeelis, Selective gene-expression profiling of migratory tumor cells in vivo predicts clinical outcome in breast cancer patients. *Breast Cancer Res.* **14**, R139 (2012).
32. A. C. Society, *Breast Cancer Facts & Figures 2015-2016* (American Cancer Society Inc., 2015).
33. T. Shree, O. C. Olson, B. T. Elie, J. C. Kester, A. L. Garfall, K. Simpson, K. M. Bell-McGuinn, E. C. Zabor, E. Brogi, J. A. Joyce, Macrophages and cathepsin proteases blunt chemotherapeutic response in breast cancer. *Genes Dev.* **25**, 2465–2479 (2011).
34. F. Pucci, M. A. Venneri, D. Biziato, A. Nonis, D. Moi, A. Sica, C. Di Serio, L. Naldini, M. De Palmax, A distinguishing gene signature shared by tumor-infiltrating Tie2-expressing monocytes, blood "resident" monocytes, and embryonic macrophages suggests common functions and developmental relationships. *Blood* **114**, 901–914 (2009).
35. C. Murdoch, M. Muthana, S. B. Coffelt, C. E. Lewis, The role of myeloid cells in the promotion of tumour angiogenesis. *Nat. Rev. Cancer* **8**, 618–631 (2008).
36. C. E. Lewis, A. S. Harney, J. W. Pollard, The multifaceted role of perivascular macrophages in tumors. *Cancer Cell* **30**, 18–25 (2016).
37. E. Fremder, M. Munster, A. Aharon, V. Miller, S. Gingis-Velitski, T. Voloshin, D. Alishekevitz, R. Bril, S. J. Scherer, D. Loven, B. Brenner, Y. Shaked, Tumor-derived microparticles induce bone marrow-derived cell mobilization and tumor homing: A process regulated by osteopontin. *Int. J. Cancer* **135**, 270–281 (2014).
38. C. L. Forse, S. Agarwal, D. Pinnaduwage, F. Gertler, J. S. Condeelis, J. Lin, X. Xue, K. Johung, A. M. Mulligan, T. E. Rohan, S. B. Bull, I. L. Andrulis, Mena^{calc}, a quantitative method of metastasis assessment, as a prognostic marker for axillary node-negative breast cancer. *BMC Cancer* **15**, 483 (2015).
39. S. Agarwal, F. B. Gertler, M. Balsamo, J. S. Condeelis, R. L. Camp, X. Xue, J. Lin, T. E. Rohan, D. L. Rimm, Quantitative assessment of invasive mena isoforms (Mena^{calc}) as an independent prognostic marker in breast cancer. *Breast Cancer Res.* **14**, R124 (2012).
40. M. J. Oudin, S. K. Hughes, N. Rohani, M. N. Moufarrej, J. G. Jones, J. S. Condeelis, D. A. Lauffenburger, F. B. Gertler, Characterization of the expression of the pro-metastatic Mena^{INV} isoform during breast tumor progression. *Clin. Exp. Metastasis* **33**, 249–261 (2016).
41. G. Bonadonna, A. Moliterni, M. Zambetti, M. G. Daidone, S. Pilotti, L. Gianni, P. Valagussa, 30 years' follow up of randomised studies of adjuvant CMF in operable breast cancer: Cohort study. *BMJ* **330**, 217 (2005).
42. G. Bonadonna, E. Brusamolino, P. Valagussa, A. Rossi, L. Brugnatelli, C. Brambilla, M. De Lena, G. Tancini, E. Bajetta, R. Musumeci, U. Veronesi, Combination chemotherapy as an adjuvant treatment in operable breast cancer. *N. Engl. J. Med.* **294**, 405–410 (1976).
43. J. M. Roodhart, M. H. Langenberg, J. S. Vermaat, M. P. Lolkema, A. Baars, R. H. Giles, E. O. Witteveen, E. E. Voest, Late release of circulating endothelial cells and endothelial progenitor cells after chemotherapy predicts response and survival in cancer patients. *Neoplasia* **12**, 87–94 (2010).
44. D. G. DeNardo, D. J. Brennan, E. Rexhepaj, B. Ruffell, S. L. Shiao, S. F. Madden, W. M. Gallagher, N. Wadhwani, S. D. Keil, S. A. Junaid, H. S. Rugo, E. S. Hwang, K. Jirström, B. L. West, L. M. Coussens, Leukocyte complexity predicts breast cancer survival and functionally regulates response to chemotherapy. *Cancer Discov.* **1**, 54–67 (2011).
45. C. Murdoch, S. Tazzyman, S. Webster, C. E. Lewis, Expression of Tie-2 by human monocytes and their responses to angiopoietin-2. *J. Immunol.* **178**, 7405–7411 (2007).
46. M. A. Venneri, M. De Palma, M. Ponzoni, F. Pucci, C. Scielzo, E. Zonari, R. Mazzieri, C. Doglioni, L. Naldini, Identification of proangiogenic TIE2-expressing monocytes (TEMs) in human peripheral blood and cancer. *Blood* **109**, 5276–5285 (2007).
47. M. De Palma, L. Naldini, Angiopoietin-2 TIEs up macrophages in tumor angiogenesis. *Clin. Cancer Res.* **17**, 5226–5232 (2011).
48. C. E. Lewis, A. S. Harney, J. W. Pollard, The multifaceted role of perivascular macrophages in tumors. *Cancer Cell* **30**, 365 (2016).
49. M. J. Oudin, L. Barbier, C. Schäfer, T. Kosciuk, M. A. Miller, S. Han, O. Jonas, D. A. Lauffenburger, F. B. Gertler, MENA confers resistance to paclitaxel in triple-negative breast cancer. *Mol. Cancer Ther.* **16**, 143–155 (2017).
50. S. K. Swisher, J. Vila, S. L. Tucker, I. Bedrosian, S. F. Shaitelman, J. K. Litton, B. D. Smith, A. S. Caudle, H. M. Kuerer, E. A. Mittendorf, Locoregional control according to breast cancer subtype and response to neoadjuvant chemotherapy in breast cancer patients undergoing breast-conserving therapy. *Ann. Surg. Oncol.* **23**, 749–756 (2016).
51. F. M. Blows, K. E. Driver, M. K. Schmidt, A. Broeks, F. E. van Leeuwen, J. Wesseling, M. C. Cheang, K. Gelmon, T. O. Nielsen, C. Blomqvist, P. Heikkilä, T. Heikkinen, H. Nevanlinna, L. A. Akslen, L. R. Bégin, W. D. Foulkes, F. J. Couch, X. Wang, V. Cafourek, J. E. Olson, L. Baglietto, G. G. Giles, G. Severi, C. A. McLean, M. C. Southey, E. Rakha, A. R. Green, I. O. Ellis, M. E. Sherman, J. Lissowska, W. F. Anderson, A. Cox, S. S. Cross, M. W. R. Reed, E. Provenzano, S.-J. Dawson, A. M. Dunning, M. Humphreys, D. F. Easton, M. García-Closas, C. Caldas, P. D. Pharoah, D. Huntsman, Subtyping of breast cancer by immunohistochemistry to investigate a relationship between subtype and short and long term survival: A collaborative analysis of data for 10,159 cases from 12 studies. *PLOS Med.* **7**, e1000279 (2010).
52. L. Zhang, S. Riethdorf, G. Wu, T. Wang, K. Yang, G. Peng, J. Liu, K. Pantel, Meta-analysis of the prognostic value of circulating tumor cells in breast cancer. *Clin. Cancer Res.* **18**, 5701–5710 (2012).
53. J.-Y. Pierga, F.-C. Bidard, C. Mathiot, E. Brain, S. Delaloge, S. Giachetti, P. de Cremoux, R. Salmon, A. Vincent-Salomon, M. Marty, Circulating tumor cell detection predicts early metastatic relapse after neoadjuvant chemotherapy in large operable and locally advanced breast cancer in a phase II randomized trial. *Clin. Cancer Res.* **14**, 7004–7010 (2008).
54. W. Onstenk, J. Kraan, B. Mostert, M. M. Timmermans, A. Charehbili, V. T. H. B. M. Smit, J. R. Kroep, J. W. R. Nortier, S. van de Ven, J. B. Heijns, L. W. Kessels, H. W. M. van Laarhoven, M. M. E. M. Bos, C. J. H. van de Velde, J. W. Gratama, A. M. Sieuwerts, J. W. M. Martens, J. A. Foekens, S. Sleijfer, Improved circulating tumor cell detection by a combined EpCAM and MCAM CellSearch enrichment approach in patients with breast cancer undergoing neoadjuvant chemotherapy. *Mol. Cancer Ther.* **14**, 821–827 (2015).
55. C. T. Guy, R. D. Cardiff, W. J. Muller, Induction of mammary tumors by expression of polyomavirus middle T oncogene: A transgenic mouse model for metastatic disease. *Mol. Cell. Biol.* **12**, 954–961 (1992).
56. F. Ahmed, J. Wyckoff, E. Y. Lin, W. Wang, Y. Wang, L. Hennighausen, J.-i. Miyazaki, J. Jones, J. W. Pollard, J. S. Condeelis, J. E. Segall, GFP expression in the mammary gland for imaging of mammary tumor cells in transgenic mice. *Cancer Res.* **62**, 7166–7169 (2002).
57. D. Entenberg, J. Wyckoff, B. Gligorijevic, E. T. Roussos, V. V. Verkhusha, J. W. Pollard, J. Condeelis, Setup and use of a two-laser multiphoton microscope for multichannel intravital fluorescence imaging. *Nat. Protoc.* **6**, 1500–1520 (2011).
58. D. Entenberg, D. Kedrin, J. Wyckoff, E. Sahai, J. Condeelis, J. E. Segall, Imaging tumor cell movement in vivo. *Curr. Protoc. Cell Biol.* **Chapter 19**, Unit 19.7 (2013).
59. C. A. Schneider, W. S. Rasband, K. W. Eliceiri, NIH Image to ImageJ: 25 years of image analysis. *Nat. Methods* **9**, 671–675 (2012).
60. J. B. Wyckoff, J. G. Jones, J. S. Condeelis, J. E. Segall, A critical step in metastasis: In vivo analysis of intravasation at the primary tumor. *Cancer Res.* **60**, 2504–2511 (2000).
61. P. Thevenaz, U. E. Ruttimann, M. Unser, A pyramid approach to subpixel registration based on intensity. *IEEE Trans. Image Process.* **7**, 27–41 (1998).
62. P. J. Boimel, T. Smirnova, Z. N. Zhou, J. Wyckoff, H. Park, S. J. Coniglio, B.-Z. Qian, E. R. Stanley, D. Cox, J. W. Pollard, W. J. Muller, J. Condeelis, J. E. Segall, Contribution of CXCL12 secretion to invasion of breast cancer cells. *Breast Cancer Res.* **14**, R23 (2012).
63. H. Gil-Henn, A. Patsialou, Y. Wang, M. S. Warren, J. S. Condeelis, A. J. Koleske, Arg/Abl2 promotes invasion and attenuates proliferation of breast cancer in vivo. *Oncogene* **32**, 2622–2630 (2013).
64. T. D. Schmittgen, K. J. Livak, Analyzing real-time PCR data by the comparative C_T method. *Nat. Protoc.* **3**, 1101–1108 (2008).

65. M. D. Weidmann, C. R. Surve, R. J. Eddy, X. Chen, F. B. Gertler, V. P. Sharma, J. S. Condeelis, Mena^{INV} dysregulates cortactin phosphorylation to promote invadopodium maturation. *Sci. Rep.* **6**, 36142 (2016).

Acknowledgments: We thank the Histopathology Core Facility in the Albert Einstein College of Medicine for assistance in IHC and the Analytical Imaging Facility for assistance in imaging and microscopy. We also thank R. Eddy and M. Chen for the development and validation of the MENA^{INV} antibody, J. Lin for help with selected data analysis, and Y. Lin for technical assistance. We finally thank Deciphera Pharmaceuticals for providing rebastinib for the experiments described in Fig. 8. **Funding:** Our work is supported by grants from the NIH (CA100324, CA150344, and 1T32CA200561-01), the T32 Research Training Grant of Surgeons, the SIG 1S10OD019961-01, the Gruss Lipper Biophotonics Center, and the Integrated Imaging Program at the Albert Einstein College of Medicine. **Author contributions:** G.S.K. designed and performed the experiments, analyzed and interpreted the data, coordinated the project, and co-wrote the manuscript. J.M.P. performed IVI experiments. Y.W. performed animal handling. A.S.H. and E.A.X. performed IF imaging. D.E. developed image analysis software and performed IVI. V.P.S. contributed HyperStackReg plug-in for image alignment in intravital movies and helped define methodology for generating vascular permeability exclusion masks in ImageJ. J.P. performed qRT-PCR for *MENA^{INV}* in patient FNA biopsies. J.G.J. analyzed TMEM triple staining. J.A., E.C., T.M.D., and J.A.S. provided human samples for histopathology. T.E.R. contributed to data interpretation. J.S.C. guided multiphoton imaging and IF data interpretation. M.H.O. guided histology and IHC experiments (TMEM triple staining). J.S.C. and M.H.O. conceived the hypothesis, led the project, interpreted the data, and wrote the manuscript. **Competing interests:** J.S.C. and M.H.O. are inventors on a patent application (#96700/2505) submitted by Albert Einstein College of Medicine that covers methods of detecting and reducing chemotherapy-induced prometastatic changes in breast tumors. All other authors declare that they have no competing interests.

Submitted 20 February 2017
Accepted 13 June 2017
Published 5 July 2017
10.1126/scitranslmed.aan0026

Citation: G. S. Karagiannis, J. M. Pastoriza, Y. Wang, A. S. Harney, D. Entenberg, J. Pignatelli, V. P. Sharma, E. A. Xue, E. Cheng, T. M. D'Alfonso, J. G. Jones, J. Anampa, T. E. Rohan, J. A. Sparano, J. S. Condeelis, M. H. Oktay, Neoadjuvant chemotherapy induces breast cancer metastasis through a TMEM-mediated mechanism. *Sci. Transl. Med.* **9**, eaan0026 (2017).